Table 1. Continued.

Clinical feature	Patient number 1	2	3	4	5	6	7	8	9	10	11
Abrupt diffuse attenuation of background activity on EEG	+	+	–	–	+	–	+	+	–	–	+
Seizure frequency	≥1/day	≥1/day	≥1/day	0–2/day (TS)	>50/day	10/day	Peak 30–50/day	5/day (TS)	10/day	>20/day	Peak 200/day
Temporarily effective drugs	PB, KD, CBZ	High-dose PB, LEV, KD, LTG	VPA, PB, TPM	VPA, PB, LTG, LEV, KD	PB, TPM, KD	CZP, CLB, PB, PHT, LEV	ZNS, PB, CZP, PHT, TPM, ST, KBr	VGB	CLB, PB, PHT, NaBr, MDL	LEV, KD	KD
Ineffective drugs	KBr, TPM VitB6	PB, CLB VitB6, LEU	VitB6, ZNS, CZP, ACTH, PHT	VitB6, CZP, CBZ, PHT, TPM, LD, IVIG, Steroid pulse	VPA, CBZ, KBr, LEV, VitB6	VitB6, ZNS	VitB6, corpus callosotomy	VitB6, ACTH, VPA, ZNS, TPM, LTG, LEV	CBZ, ZNS, LEV, LD	ACTH, VPA, CLB, CZP, PB, CBZ, ZNS, KBr	CBZ, VPA, CLB, PHT, ZNS, GBP, LTG, LEV, KBr
ID	+	+	+	+	+	+	+	+	+	+	+
Muscle tonus	Normal or spasticity	Spasticity → hypotonia		Spasticity	Spasticity→ hypotonia						Mild hypotonia
Involuntary movements	–	–	–	Chorea (left fingertip)	–	–	–	–	–	–	–
Current status	Bedridden	Bedridden	Bedridden	Bedridden	Bedridden	Bedridden	Bedridden	Bedridden	Bedridden	Bedridden	Bedridden
Brain MRI	Thin CC at 2 mo, delayed myelination, CA at 10 mo	Normal at 28 days, thin CC at 7 mo, diffuse CA and delayed myelination at 35 mo	Mildly thin CC and CA at 2 mo, and subdural hematoma at 4 mo	Subdural hygroma at 4 mo, diffuse CA at 7 mo	Normal at 2 mo, CA at 1 y	Normal at 2 mo and 2 y	Normal at 7 mo except for disconnected CC	Normal at 3 mo, diffuse CA at 20 mo	Normal at 2 mo	Normal at 1 and 2 mo	Normal at 1 mo, hypoplastic CC, delayed myelination, and left lateral ventricular dilatation

y, years; mo, months; EIMFS, epilepsy of infancy with migrating focal seizures; OS, Ohtahara syndrome; West, West syndrome; EOEE, early onset epileptic encephalopathies; ID, intellectual disability; TS, tonic seizure; sp-w, spike and slow wave; SB, suppression-burst; Hyps, hypsarrhythmia; MFS, multifocal spike; PB, phenobarbital; KD, ketogenic diet; CBZ, carbamazepine; LEV, levetiracetam; LTG, lamotrigine; VPA, valproic acid; TPM, topiramate; CZP, clonazepam; CLB, clobazam; PHT, phenytoin; ZNS, zonisamide; ST, sodium thiamylal; KBr, potassium bromide; VGB, vigabatrin; NaBr, sodium bromide; MDL, midazolam; VitB6, vitamin B6; LEU, leucovorin; LD, lidocaine; IVIG, intravenous immunoglobulin; ACTH, adrenocorticotrophic hormone; GBP, gabapentin; CC, corpus callosum; CA, cerebral atrophy.

[a]Inherited from the mother who carried a somatic mosaic mutation.

Epilepsia, 56(9):e121–e128, 2015
doi: 10.1111/epi.13072

EIMFS is characterized by migrating polymorphous focal seizures starting within the first 6 months of life, followed by progressive deterioration of psychomotor development and resistance to antiepileptic drugs.[3]

KCNT1 encodes the Na^+-activated K^+ channel known as Slack, Slo2.2, or KCa4.1.[4,5] KCNT1 (Slack) consists of six transmembrane segments (S1–S6) with a pore P-domain between S5 and S6 and a large cytoplasmic C-terminal domain containing two regulators of K^+ conductance (RCK) domains.[5] KCNT1 is expressed in adult rat brain, especially in the cortex and hippocampus, and in embryonic hippocampal and cortical mouse neurons.[4–6] De novo *KCNT1* mutations resulting in an increase in K^+ current amplitude have recently been identified in patients with EIMFS.[7–9] Furthermore, *KCNT1* mutations were found in patients with autosomal dominant nocturnal frontal lobe epilepsy (ADNFLE), intellectual disability, and psychiatric problems,[10] and in a patient with leukoencephalopathy and severe epilepsy.[11] A homozygous *KCNT1* mutation was also identified in a patient with OS,[12] suggesting a wide phenotypic spectrum of *KCNT1* mutations.

In this study, we performed *KCNT1*-targeted next-generation sequencing and/or focused *KCNT1* analysis using whole-exome sequencing (WES). We identified *KCNT1* mutations in 11 patients with EOEE and analyzed their clinical phenotypes.

Methods

A total of 362 patients with EOEE (98 patients with OS, 180 with West syndrome, 18 with EIMFS, and 66 with unclassified EOEEs with an onset age of <1 year) were analyzed. Diagnoses were made on the basis of clinical features and electroencephalography (EEG) patterns. Detailed clinical information was obtained from corresponding clinicians.

We performed *KCNT1*-targeted next-generation sequencing of 207 patients using polymerase chain reaction (PCR) amplification of all *KCNT1* exons on the MiSeq platform (Illumina, San Diego, CA, U.S.A.) (see Data S1 and Table S1). This identified one patient with a *KCNT1* mutation. In 74 of 206 patients who were negative for *KCNT1* mutations and for whom sufficient amounts of DNA were available for further analysis, we performed WES as described previously (see Data S1 for more details).[13] To expand our cohort we then added 155 patients, who were examined by WES as the first screening method. As a result, a total of 229 patients were examined by WES. Of these, 51 patients were shown to carry mutations in known epilepsy genes other than *KCNT1*, whereas 10 harbored *KCNT1* mutations. The total number of patients with *KCNT1* mutations was therefore 11/362 (3.0%, Fig. S1).

Experimental protocols were approved by the institutional review board of Yokohama City University School of Medicine and Yamagata University Faculty of Medicine. Written informed consent was obtained from all individuals and/or their families in compliance with relevant Japanese regulations.

Results

Clinical features of patients with *KCNT1* mutations

Nine different *KCNT1* mutations were found in 11 patients: in 9 (50%) of 18 EIMFS cases, one (0.56%) of 180 West syndrome cases, and one (1.52%) of 66 unclassified EOEE cases. The clinical features of the 11 patients with *KCNT1* mutations are summarized in Table 1. Most patients with *KCNT1* mutations were diagnosed with EIMFS (9/11) because alternating seizures accompanied by shifting or migrating foci from one area to another were recognized on electroencephalography (EEG; Fig. S2). In these nine patients with EIMFS, onset ages were within 4 months after birth, and interictal EEG showed multifocal spikes. Four of the nine patients had additional EEG findings, such as an abrupt diffuse attenuation of background activity consisting of a brief period of suppression (flat phase ≥3 s) in patients 1, 2, and 5 (Fig. 1) or hypsarrhythmia with desynchronization (flat phase <3 s) in patients 5 and 7, as reported previously in patients with EIMFS.[3] Brain magnetic resonance imaging (MRI) revealed abnormalities of the corpus callosum in four patients (4/9), cerebral atrophy in five (5/9), and delayed myelination in two (2/9) (Fig. S3). All these children showed motor and cognitive impairment and intractable seizures occurred >10 times/day in five patients (5/9).

Patient 8 with West syndrome showed epileptic spasms in clusters and hypsarrhythmia on EEG at 2 and 3 months of age, respectively. Focal seizures were not observed. Patient 11 with unclassified EOEE demonstrated frequent seizures comprising staring and bilateral clonic or right hemiclonic convulsions at 1 month, but he showed neither epileptic spasms nor migrating focal seizures. In these two cases, EEG also showed an abrupt diffuse attenuation of background activity consisting of hypsarrhythmia with desynchronization (patient 8) or a brief period of suppression (patient 11). Brain MRI revealed cerebral atrophy in patient 8, and a thin corpus callosum and delayed myelination in patient 11. The case reports for these two patients are available in Data S2.

All 11 patients with *KCNT1* mutations were bedridden (at ages of 1–6 years). Various antiepileptic treatments were only temporarily effective at controlling seizures: phenobarbital (PB) or high-dose PB maintaining a blood level of >40 μg/ml in eight patients and a ketogenic diet in six, whereas vitamin B6 (eight patients), zonisamide (six patients), carbamazepine (five patients), and potassium bromide, topiramate, and levetiracetam (LEV) (four patients) were ineffective.

Characterization of *KCNT1* mutations

Among 11 patients with *KCNT1* mutations, one was identified by *KCNT1*-targeted next-generation sequencing and

the others were identified by WES; sufficient depth of coverage was obtained in both techniques (Fig. S1). In 10 cases analyzed by WES, no other mutations were found in 20 known epilepsy genes, including *SCN8A*, *FOXG1*, *KCNQ2*, *SCN1A*, *SCN2A*, *STXBP1*, *SPTAN1*, *CDKL5*, *PCDH19*, *MECP2*, *GNAO1*, *CASK*, *SLC35A2*, *ALG13*, *GABRB3*, *HDAC4*, *DNM1*, *CHD2*, *SYNGAP1*, and *GRIN2A*, except for a *GABRB3* [c.17T>C (p.L6P)] variant in patient 10 and a *KCNQ2* [c.2594T>G (p.V865G)] variant in patient 11; both of these variants were inherited from the unaffected father (Table S2). All other *KCNT1* mutations, apart from one (c.2771C>T), occurred de novo. High-resolution melting analysis suggested that the c.2771C>T mutation was transmitted from the patient's unaffected mother, who had a possible mosaic mutation. The mosaic mutation was confirmed by Sanger sequencing and deep sequencing of polymerase chain reaction (PCR) products amplified using DNA extracted from the mother's blood, saliva, and nails (Fig.

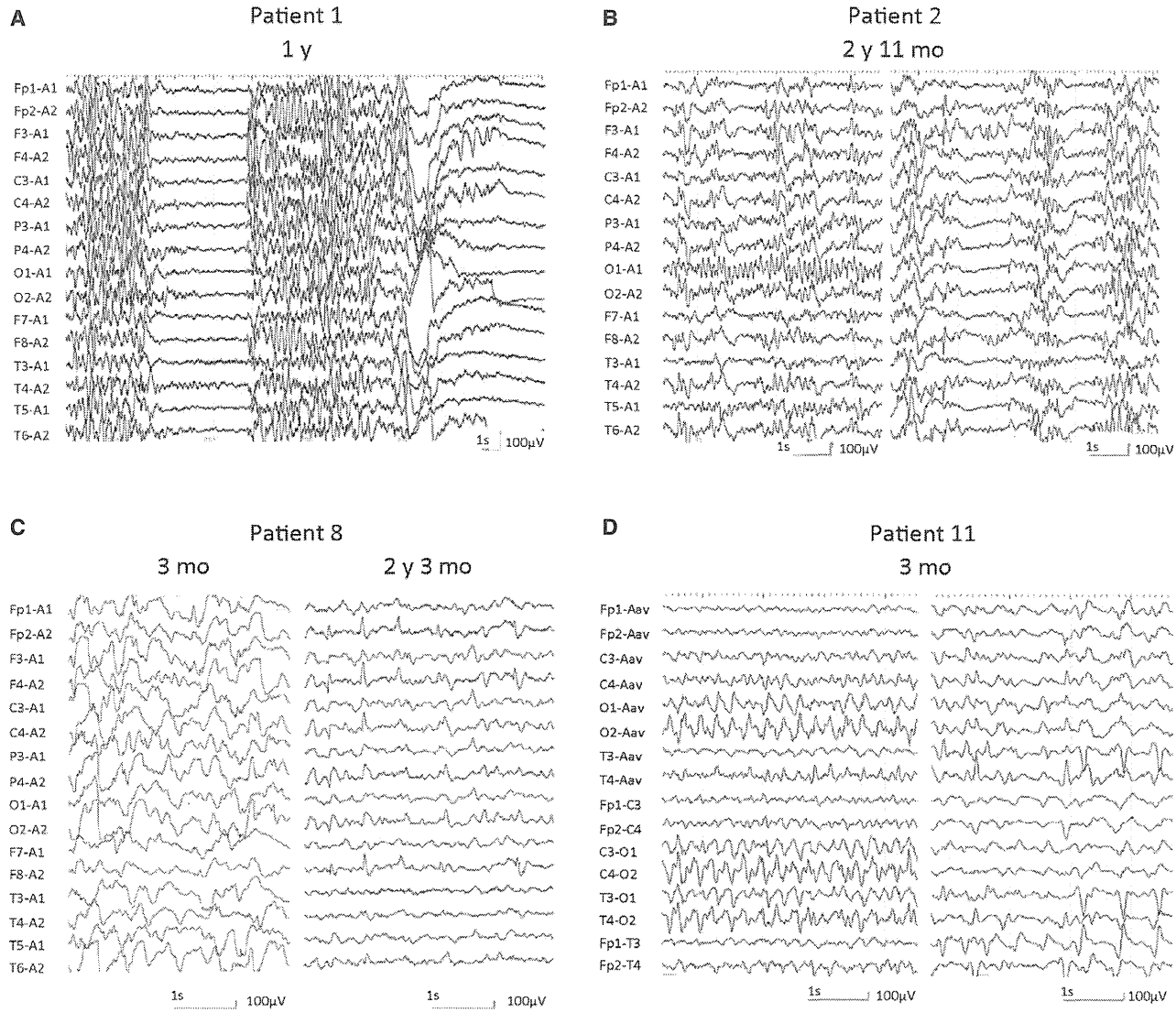

Figure 1.

EEGs of patients with *KCNT1* mutations. (**A**) EEG of patient 1 at 1 year of age showing a brief period of suppression. (**B**) EEG of patient 2 at 2 years and 11 months of age showing multifocal polyspikes or an alternate pattern of desynchronization and high-amplitude sharp waves similar to a suppression-burst pattern. (**C**) EEG studies of patient 8 at 3 months of age (left panel) showing multifocal sharp waves with high-amplitude irregular slow waves consistent with a finding of hypsarrhythmia, and at 2 years and 3 months (right panel) showing focal spikes. (**D**) Ictal EEG of patient 11 at 3 months of age (left panel) showing rhythmic delta-wave activity in the bilateral occipital area with a right-sided predominance. Interictal EEG (right panel) shows multifocal sharp waves. The horizontal calibration bar indicates 1 s and the vertical bar indicates 100 μV. y, years; mo, months.

S4: mutant allele frequency range, 14–29%). All nine mutations were absent from the 6,500 exomes included in the National Heart, Lung, and Blood Institute exome project and from our 575 in-house control exomes. Sorting Intolerant from Tolerant (SIFT), Polyphen2, and Mutation Taster predicted all mutations to be highly damaging to the structure of KCNT1, and all mutations occurred at evolutionarily conserved amino acids (Table S2 and Fig. S5). Schematic presentation of the mutations in human KCNT1[6,14] revealed that they accumulated in the S5 and RCK domains 1 and 2 (Fig. 2): two mutations were located in S5 (2/9, 22.2%), five mutations were located in RCK domain 1 (5/9, 55.6%), and two were located in RCK domain 2 (2/9, 22.2%). An Arg474 residue in RCK domain 1 was mutated in four patients: c.1420C>T (p.R474C) in patient 1 and c.1421G>A (p.R474H) in patients 5, 7, and 8 (Fig. 2 and Table 1). Five of nine mutations were recurrent (p.G288S, p.R428Q, p.R474H, p.P924L, and p.A934T), and have been reported previously in patients with EIMFS.[7–9]

Discussion

Our results demonstrate that *KCNT1* mutations are strongly associated with EIMFS because 9 (81%) of 11

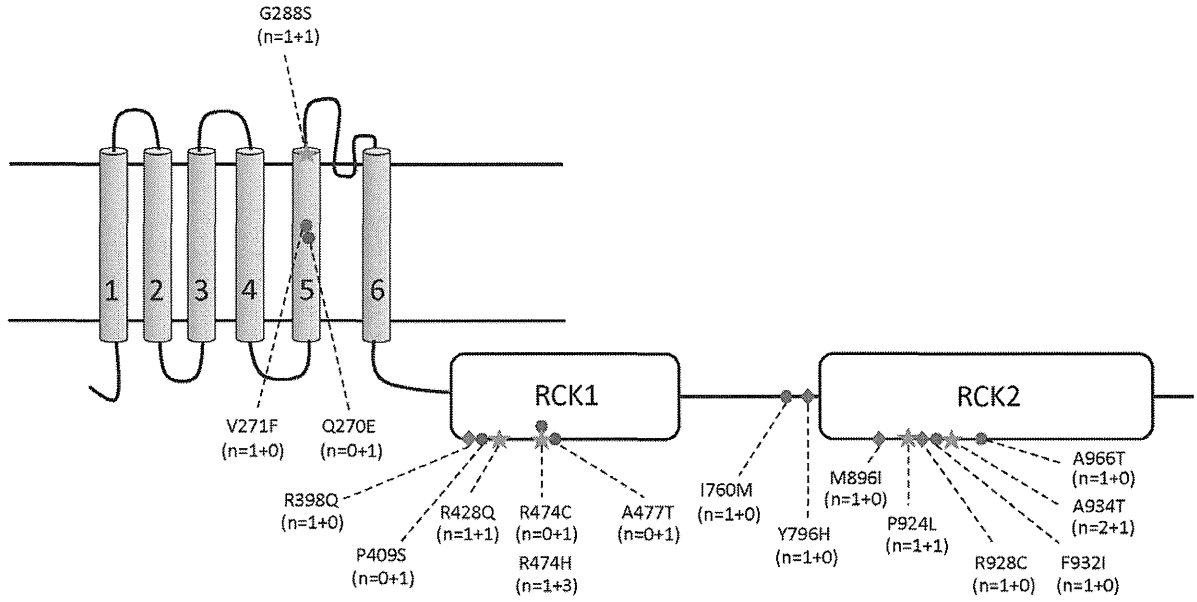

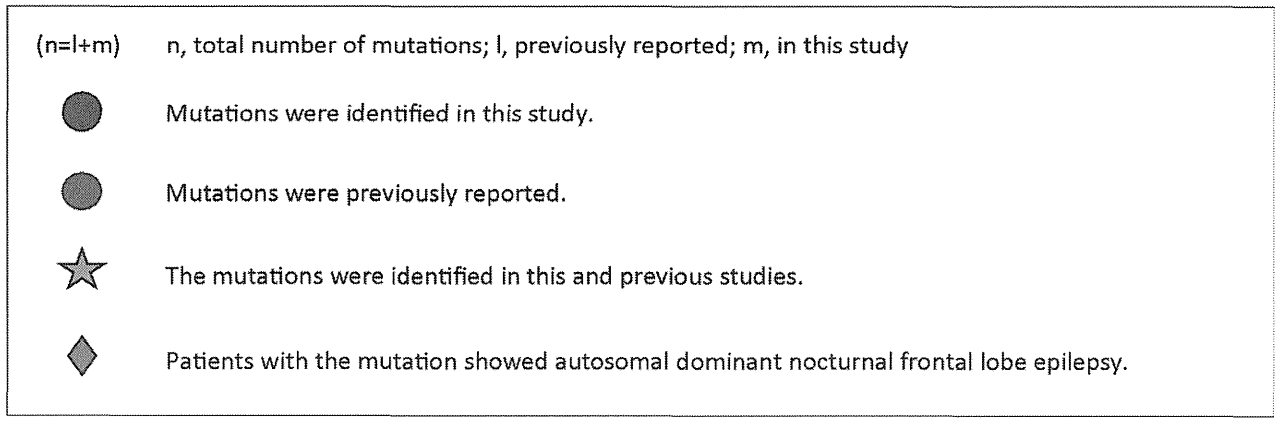

Figure 2.
Schematic presentation of human KCNT1 protein and *KCNT1* mutations. Mutations are annotated on the basis of NM_020822.2. p.V271F, p.G288S, p.R428Q, p.R474H, p.I760M, p.P924L, and p.A934T were previously reported in patients with EIMFS.[3,7–9] p.R398Q, p.Y796H, p.M896I, and p.R928C were reported in patients with ADNFLE.[10] p.F932I was reported in patients with leukoencephalopathy and severe epilepsy.[11] A homozygous p.A966T mutation was reported in a patient with OS.[12] n, total number of mutations, l = previously reported mutation; m, mutation found in this study.
Epilepsia © ILAE

patients harboring these mutations were diagnosed with EIMFS and presented with ictal discharges on EEG occurring in one region and shifting (migrating) to another with clinical seizures (patients 1, 3, 4, 5, 6, 7, and 10) or without clinical seizures (patients 2 and 9). This compares with a *KCNT1* mutation being detected in only one of 180 patients with West syndrome who showed characteristic epileptic spasms, and in one of 66 cases with unclassified EOEE. Among 11 patients with *KCNT1* mutations, only these two patients showed no shifting (migrating) ictal or subclinical discharges from one area to another. However, focal seizures and independent multifocal spikes, which did not overlap (so were not migrating), were seen even in the patient with unclassified EOEE. Focal discharges and seizures are highly likely to be characteristic of the phenotype associated with *KCNT1* mutations because they are also seen in patients with ADNFLE caused by *KCNT1* mutations.[10] Although no *KCNT1* mutations were found in 98 patients with typical OS, suppression-burst–like activity was seen in four patients (patients 1, 2, 5, and 11), which was previously reported in one of 14 patients with EIMFS.[3] Moreover, desynchronization with or without hypsarrhythmia was seen in three patients (patients 5, 7, and 8). Patient 5 also demonstrated suppression-burst-like activity. In total, 6 of 11 cases showed electrodecremental discharges on EEG, which is supportive of these being another characteristic feature for *KCNT1* mutation phenotypes, as reported previously.[3]

The patient with West syndrome (patient 8) carried the recurrent mutation (c.1421G>A) as did the patients with EIMFS, and we observed no genotype–phenotype correlation with *KCNT1* mutations. Although the frequency of *KCNT1* mutations among patients with West syndrome is low, the genetic background for West syndrome or infantile spasms is heterogeneous, suggesting that *KCNT1* should be included on the list of causative genes for West syndrome.

All patients with *KCNT1* mutations in the current study had intractable seizures that were only temporarily controlled by antiepileptic treatments. The development of novel therapies or identification of effective agents is thus crucial. A recent report suggested that the antiarrhythmic drug quinidine was able to reverse mutation-specific gain-of-function properties.[15] Although it is necessary to consider possible adverse effects, quinidine may represent a promising targeted therapy for patients with *KCNT1* mutations.

In conclusion, we identified nine *KCNT1* mutations in 11 patients, of whom nine were compatible with EIMFS. This indicates that the phenotypic spectrum of de novo *KCNT1* mutations is largely restricted to EIMFS. Moreover, electrodecremental discharges on EEG are an additional characteristic feature of the *KCNT1* mutation phenotype.

Acknowledgments

We are grateful to the patients and their families for their participation in this study. We thank Nobuko Watanabe, Kiyomi Masuko, and Sayaka Sasamoto for their excellent technical assistance. This work was supported by the Ministry of Health, Labour and Welfare of Japan; the Japan Society for the Promotion of Science [Grant-in-Aid for Scientific Research (B) from (25293085, 25293235), Grant-in-Aid for Scientific Research (A) (13313587), and Grant-in-Aid for Scientific Research (C) (24591500)]; the Takeda Science Foundation; the Fund for Creation of Innovation Centers for Advanced Interdisciplinary Research Areas Program in the Project for Developing Innovation Systems (N. Matsumoto) from the Japan Science and Technology Agency; the Strategic Research Program for Brain Sciences (11105137); and a Grant-in-Aid for Scientific Research on Innovative Areas (Transcription Cycle) from the Ministry of Education, Culture, Sports, Science and Technology of Japan (12024421).

Disclosure

None of the authors has any conflict of interest to disclose. We confirm that we have read the journal's position on issues involved in ethical publication and affirm that this report is consistent with those guidelines.

References

1. Mastrangelo M, Leuzzi V. Genes of early-onset epileptic encephalopathies: from genotype to phenotype. *Pediatr Neurol* 2012;46:24–31.
2. Berg AT, Berkovic SF, Brodie MJ, et al. Revised terminology and concepts for organization of seizures and epilepsies: report of the ILAE Commission on Classification and Terminology, 2005–2009. *Epilepsia* 2010;51:676–685.
3. McTague A, Appleton R, Avula S, et al. Migrating partial seizures of infancy: expansion of the electroclinical, radiological and pathological disease spectrum. *Brain* 2013;136:1578–1591.
4. Igelstrom KM. Is slack an intrinsic seizure terminator? *Neuroscientist* 2013;19:248–254.
5. Kaczmarek LK. Slack, slick and sodium-activated potassium channels. *ISRN Neurosci* 2013;2013:pii354262.
6. Joiner WJ, Tang MD, Wang LY, et al. Formation of intermediate-conductance calcium-activated potassium channels by interaction of Slack and Slo subunits. *Nat Neurosci* 1998;1:462–469.
7. Barcia G, Fleming MR, Deligniere A, et al. *De novo* gain-of-function *KCNT1* channel mutations cause malignant migrating partial seizures of infancy. *Nat Genet* 2012;44:1255–1259.
8. Ishii A, Shioda M, Okumura A, et al. A recurrent *KCNT1* mutation in two sporadic cases with malignant migrating partial seizures in infancy. *Gene* 2013;531:467–471.
9. Allen AS, Berkovic SF, Cossette P, et al. *De novo* mutations in epileptic encephalopathies. *Nature* 2013;501:217–221.
10. Heron SE, Smith KR, Bahlo M, et al. Missense mutations in the sodium-gated potassium channel gene *KCNT1* cause severe autosomal dominant nocturnal frontal lobe epilepsy. *Nat Genet* 2012;44:1188–1190.
11. Vanderver A, Simons C, Schmidt JL, et al. Identification of a novel de novo p.Phe932Ile KCNT1 mutation in a patient with leukoencephalopathy and severe epilepsy. *Pediatr Neurol* 2014;50:112–114.
12. Martin HC, Kim GE, Pagnamenta AT, et al. Clinical whole-genome sequencing in severe early-onset epilepsy reveals new genes and improves molecular diagnosis. *Hum Mol Genet* 2014;23:3200–3211.
13. Saitsu H, Nishimura T, Muramatsu K, et al. *De novo* mutations in the autophagy gene *WDR45* cause static encephalopathy of childhood with neurodegeneration in adulthood. *Nat Genet* 2013;45:445–449, 449e441.
14. Yuan P, Leonetti MD, Pico AR, et al. Structure of the human BK channel Ca^{2+}-activation apparatus at 3.0 A resolution. *Science* 2010;329:182–186.

15. Milligan CJ, Li M, Gazina EV, et al. *KCNT1* gain-of-function in two epilepsy phenotypes is reversed by quinidine. *Ann Neurol* 2014; 75:581–590.

Supporting Information

Additional Supporting Information may be found in the online version of this article:

Data S1. Methods.

Data S2. Case reports.

Figure S1. Flow chart of genetic analysis.

Figure S2. Ictal EEG of a shifting phase in patient 3 at 2 months of age.

Figure S3. T_2-weighted axial brain MRI of patients with *KCNT1* mutations.

Figure S4. Somatic mosaicism of the c.2771C>T mutation in the unaffected mother.

Figure S5. Evolutionary conservation of substituted amino acids encoded by *KCNT1* mutations.

Table S1. Primers and PCR conditions.

Table S2. Prediction of mutation pathogenicity.

PEDIATRICS INTERNATIONAL Official Journal of the Japan Pediatric Society

Pediatrics International (2015) **57**, e1–e3 doi: 10.1111/ped.12457

Patient Report

Early intervention for late-onset ornithine transcarbamylase deficiency

Daisuke Fujisawa,[1] Hiroshi Mitsubuchi,[1] Shirou Matsumoto,[1] Masanori Iwai,[1] Kimitoshi Nakamura,[1] Ryuji Hoshide,[1] Nawomi Harada,[2] Makoto Yoshino[3] and Fumio Endo[1]

[1]*Department of Pediatrics, Kumamoto University Graduate School of Medical Sciences, Kumamoto,* [2]*Department of Pediatrics and Child Health, Kurume University of Medicine and* [3]*Division of Gene Therapy and Regenerative Medicine, Cognitive and Molecular Research Institute of Brain Diseases, Kurume University, Kurume, Japan*

Abstract We report the case of a family with late-onset ornithine transcarbamylase deficiency (OTCD). Several family members had died from OTCD, and the c.221G>A, p.Lys221Lys mutation was detected at the 3′ end of exon 6 of *OTC* in the X-chromosome of some members. We provided genetic counseling on pregnancy, delivery, and neonate management to a 4th-generation female carrier and decided on metabolic management of her child from birth. Two male patients were diagnosed with late-onset OTCD on the basis of blood amino acid and genetic analysis, and they received arginine supplementation from the asymptomatic, early neonatal period. These children grew and developed normally, without decompensation. Patients with late-onset OTCD can and should be diagnosed and treated in the early neonatal period, especially those from families already diagnosed with late-onset OTCD, and family members must be provided with genetic counseling.

Key words arginine supplementation, blood amino acid analysis, genetic analysis, genetic counseling, late-onset ornithine transcarbamylase deficiency.

Ornithine transcarbamylase deficiency (OTCD) is one of the most common urea cycle disorders, with an estimated prevalence of 1 per 80 000 births. It is transmitted as an X-linked trait and the gene responsible for it, namely, *OTC*, is located on locus Xp21.1.[1] A remarkable feature of OTCD is that the phenotype is extremely heterogenous.[2,3]

Male neonates with OTCD often suffer from ammonia toxicity, protein intolerance, and death within 1 week after birth. Those with late-onset OTCD (age at onset, ≥28 days), however, have several, wide-ranging symptoms, from asymptomatic phenotype to hyperammonemia, coma, and death.[1,4,5] In heterozygous female neonates, one allele of *OTC* on the X-chromosome is silenced because of X-inactivation, and the phenotypes are varied, similar to those in male neonates with late-onset OTCD.

No reports are available on the management of asymptomatic male patients with late-onset OTCD who are diagnosed and treated early in the neonatal period. Here, we report a large pedigree involving late-onset OTCD in which male neonates were definitively diagnosed using gene and amino acid analysis soon after birth. The patients received arginine supplementation treatment, and they grew and developed well.

Correspondence: Hiroshi Mitsubuchi, MD PhD, Department of Pediatrics, Kumamoto University Graduate School of Medical Sciences, 1-1-1 Honjo, Kumamoto 860-8556, Japan. Email: mitsubuchi@fc.kuh.kumamoto-u.ac.jp

Received 27 June 2013; revised 3 July 2014; accepted 14 July 2014.

Case report

The proband (IV-19) was admitted (Fig. 1) at 7 years of age for hyperammonemia (blood ammonia, 178 μmol/L) with vomiting and coma, although his condition stabilized with intensive care. After OTC activity in the liver tissue was found to be low (0.047 μmol/mg protein/min; control, 0.96), he was prescribed oral arginine supplementation for long-term management. Because of the proband's low OTC activity, his sister underwent allopurinol test and was found to be a heterozygous carrier of the OTCD mutation. After the proband was discharged from hospital, a c.221G>A, p.Lys221Lys mutation was detected at the 3′ end of exon 6 of *OTC* in his X-chromosome, which was judged to cause a splicing abnormality (Fig. 2). Based on this finding, the proband was diagnosed with late-onset OTCD. Eight years later, the proband's 4-year-old male second cousin (IV-18) died of hyperammonemic coma (blood ammonia, >1953 μmol/L). The diagnosis of late-onset OTCD was confirmed on detection of the same mutation in the cousin.[6]Subsequently, the sisters of the deceased cousin were examined for the mutation, and were found to be heterozygous carriers.

Eleven years after the onset of OTCD in the proband, a female carrier (IV-16) of OTCD – the sister of patient IV-18 – requested genetic counseling for pregnancy and delivery, considering the family history of late-onset OTCD. The information provided included postpartum management of neonates. The carrier was informed that the mutation would manifest late-onset OTCD phenotypes in the family. We planned to analyze metabolic profiles from the early neonatal period for all this family's children born henceforth and to sequence the *OTC* gene simultaneously in these individuals.

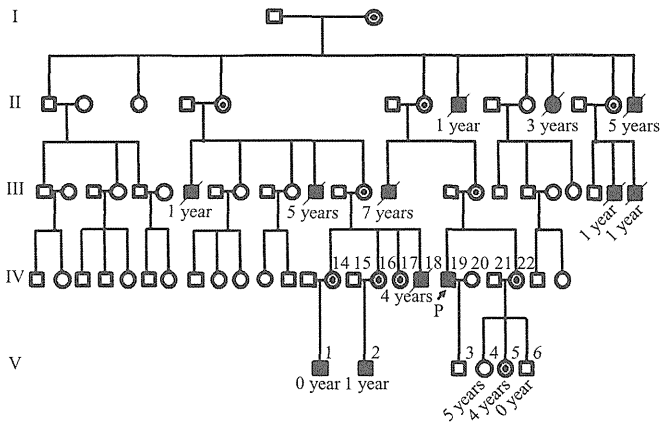

Fig. 1 Pedigree of patients with late-onset ornithine transcarbamylase (OTC) deficiency. *OTC* was analyzed in the proband (P), his two nieces (V-4, V-5) and nephew (V-6), the male member in the fourth generation who died at age 4 years with his three sisters, and two fifth-generation male infants (V-1 and V-2). The proband's sister was diagnosed on allopurinol test.

The clinical progress of patient IV-16's pregnancy was stable; the fetus was determined to be male (V-2). The baby was born at term with an Apgar score of 8/9. He started breast-feeding with his own mother's milk on the day of birth. At 3 days of age, his blood ammonium gradually increased to 91.8 μmol/L; therefore, he was started on oral arginine supplementation. At the age of 3 days the infant's blood amino acid was analyzed before arginine supplementation was started (Table 1), and slight changes were observed: glutamine increased, citrulline and arginine decreased, and ornithine remained unchanged. Urinary orotic acid was not elevated at hyperammonemia onset. The patient's blood ammonium decreased to the normal range within a few days after initiation of arginine supplementation.

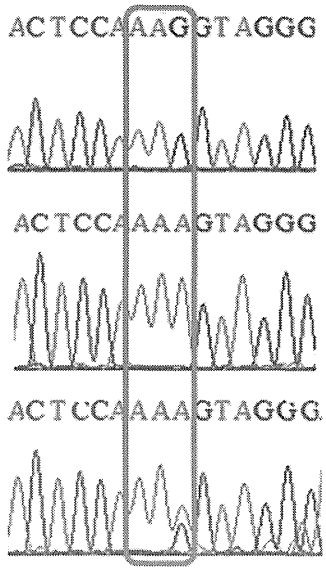

Fig. 2 *OTC* gene analysis at codon 221, exon 6 in the X-chromosome. Red line, codon 221 at the 3′ end of exon 6 of the X-chromosome. Wild-type codon 221 (upper) is AAG. In the patients, the mutation from AAG to AAA was either homozygous (middle) or heterozygous (lower).

Gene analysis conducted in the early neonatal period showed that patient V-2 (Fig. 1) had the aforementioned mutation in exon 6 of *OTC*. After 1 year, the same metabolic profile management and gene analysis were conducted in the early neonatal period for two other male infants – namely, V-1 and V-6 – and the genetic profile of the female infants – namely, V-4 and V-5 – was examined. Patient V-1 had the mutation and showed changes in blood amino acid level, similar to patient V-2. Therefore, for metabolic balance management, he also received arginine supplementation. At this time, however, the increase in urinary orotic acid could not be detected in this patient. Because low citrulline was found in the early neonatal period, the patients also received citrulline supplementation. At 2 months of age, arginine and citrulline levels improved (Table 1). The male infant V-6 did not have the mutation or the abnormal blood amino acid levels. The female infant V-5, however, was diagnosed as a carrier on genetic analysis (Fig. 1). Her blood amino acid levels were not analyzed at that time, given that she looked asymptomatic and stable.

Patients V-1 and V-2 grew well, and were followed up for a period of 1 and 2 years, respectively. They developed without decompensation during childhood and had a normal balance of arginine and glutamine, although the citrulline in V-2 remained slightly low (Table 1).

Discussion

Late-onset OTCD involves various hyperammonemic symptoms of wide-ranging severity, including vomiting, lethargy, seizures, coma, and even death. The aim of long-term management of late-onset OTCD is to improve the survival rate and maintain normal blood ammonia level and growth.[5] Patients may develop mental retardation or die when the blood ammonia exceeds 360 μmol/L.[7] Arginine is an indispensable amino acid for increasing the production of urea. Its shortage causes rapid onset of life-threatening hyperammonemia. It was found that long-term management with arginine supplementation significantly decreased the frequency of hyperammonemic attacks and improved physical growth of OTCD patients.[8] Given that it is important to prevent hyperammonemic decompensation, metabolic balance must be achieved before onset.

In addition to examination of metabolic profile, such as blood amino acid and ammonia and urinary orotic acid, mutation analysis is a very useful diagnostic tool in cases of female heterozygotes. While it is possible to predict the severity of the disease for hemizygous male patients from gene mutation analysis and/or residual enzyme activities in liver tissue, clinical features vary among female heterozygotes, because their condition is affected by not only random X-chromosome inactivation but also factors such as puberty, pregnancy, labor, delivery, and the environment.[5]We planned genetic examination of V-4, V-5 for the following reasons. First, some female carriers develop symptoms in childhood. Additionally, arginine supplementation is effective not only in the chronic phase but also in the acute phase in this large family. Therefore it is important for these female family

Table 1 Blood amino acid analysis

Amino acid (nmol/mL)	V-1†		V-2†		V-6	Reference range
	At birth	After intervention‡	At birth	After intervention‡		
Asp	3.9	6.3	6.4	11.3	3.8	≤2.4
Asn	66.3	51.6	77.4	55.3	42.2	44.7–96.8
Glu	60.2	82.6	60.1	88.3	72.9	12.6–62.5
Gln	1007.2	664.6	827	696	758.9	422.1–703.8
Ala	274.5	292.8	355.5	308	205.3	208.7–522.7
Pro	234.5	160.3	323.5	242	154.1	77.8–272.7
Val	140.1	148.8	181.2	171	117.6	147.8–307
Ile	42.8	60.6	55	73	37	43–112.8
Leu	96.4	110.1	119.1	125	82	76.6–171.3
Ornithine	68.6	115.9	91.3	103	48.4	31.3–104.7
Citrulline	4.6	22.5	5.6	7.1	20.7	17.1–42.6
Arg	38.4	121.4	37.1	108	47.6	53.6–133.6

†Ornithine transcarbamylase deficiency. ‡At 2 months of age.

members to be diagnosed as a carrier or not. Second, genetic examination is more useful than profiling of plasma amino acids for definite diagnosis of female carriers, especially when the specific mutation has been determined to be the cause of OTCD in a family. We discussed the benefits and disadvantages of the genetic diagnosis of V-4, V-5 as a definite diagnosis. Consequently, we admitted the opinion of their parents that V-4 and V-5 were examined by gene mutation analysis. The two male neonatal patients (V-1 and V-2) in this study did not have increased urinary orotic acid on gas chromatography/mass spectrometry in the early neonatal period. Blood amino acid analysis conducted simultaneously, however, provided significant information: a slight increase in glutamine and a decrease in arginine and citrulline. The high nitrogen burden causes a blood amino acid imbalance in OTCD patients. Previously, glutamine was found to have the most prominent reaction.[5]Early treatment of patient V-2 improved the amino acid balance and prevented metabolic crisis, because management was started when blood amino acid was only slightly changed and plasma ammonia was only slightly elevated. Moreover, because citrulline remained slightly low despite arginine supplementation (V-2), citrulline supplementation plays an important role in the amino acid balance (V-1). In this large pedigree, most female carriers did not show any symptoms of OTCD. Therefore, intervention with supplementation may not be necessary for some female carriers, but the outcome of these female carriers is difficult to predict. For this reason, as part of the management of the female carrier, regular profiling of her plasma amino acids is planned.

When a patient is first diagnosed with hereditary late-onset OTCD in a family, monitoring of male patients and female carriers is important so that genetic counseling can be provided, whereby it may be possible to prevent onset among family members.[4]It is vital to diagnose the condition during the asymptomatic period to prevent severe symptoms at onset.

Conclusion

Late-onset OTCD was diagnosed in asymptomatic male patients and their condition managed to prevent decompensation via treatment with arginine supplementation during the early neonatal period. The patients grew and developed well without any metabolic crises. Thus, blood amino acid and gene analysis during the early neonatal period is important for the management of families with late-onset OTCD.

References

1 Lindgren V, de Martinville B, Horwich AL, Rosenberg LE, Francke U. Human ornithine transcarbamylase locus mapped to band Xp21.1 near the Duchenne muscular dystrophy locus. *Science* 1984; **226**: 698–700.

2 Balasubramaniam S, Rudduck C, Bennetts B, Peters G, Wilcken B, Ellaway C. Contiguous gene deletion syndrome in a female with ornithine transcarbamylase deficiency. *Mol. Genet. Metab.* 2010; **99**: 34–41.

3 McCullough BA, Yudkoff M, Batshaw ML, Wilson JM, Raper SE, Tuchman M. Genotype spectrum of ornithine transcarbamylase deficiency: Correlation with the clinical and biochemical phenotype. *Am. J. Med. Genet.* 2000; **93**: 313–19.

4 Ausems MG, Bakker E, Berger R *et al.* Asymptomatic and late-onset ornithine transcarbamylase deficiency caused by a A208T mutation: Clinical, biochemical and DNA analyses in a four-generation family. *Am. J. Med. Genet.* 1997; **68**: 236–9.

5 Berry GT, Steiner RD. Long-term management of patients with urea cycle disorders. *J. Pediatr.* 2001; **138**: S56–S61.

6 Shimadzu M, Matsumoto H, Matsuura T *et al.* Ten novel mutations of the ornithine transcarbamylase (OTC) gene in OTC deficiency. *Hum. Mutat.* 1998; Suppl. 1: S5–S7.

7 Kido J, Nakamura K, Mitsubuchi H *et al.* Long-term outcome and intervention of urea cycle disorders in Japan. *J. Inherit. Metab. Dis.* 2012; **35**: 777–85.

8 Nagasaka H, Yorifuji T, Murayama K *et al.* Effects of arginine treatment on nutrition, growth and urea cycle function in seven Japanese boys with late-onset ornithine transcarbamylase deficiency. *Eur. J. Pediatr.* 2006; **165**: 618–24.

STEM CELLS

EMBRYONIC STEM CELLS/INDUCED PLURIPOTENT STEM CELLS

HPGCD Outperforms HPBCD as a Potential Treatment for Niemann-Pick Disease Type C During Disease Modeling with iPS Cells

MINAMI SOGA,[a] YOICHI ISHITSUKA,[b] MAKOTO HAMASAKI,[a] KAORI YONEDA,[c] HIROKAZU FURUYA,[d] MUNEAKI MATSUO,[e] HIRONOBU IHN,[f] NOEMI FUSAKI,[g,h] KIMITOSHI NAKAMURA,[c] NAOMI NAKAGATA,[i] FUMIO ENDO,[c] TETSUMI IRIE,[b] TAKUMI ERA[a]

[a]Department of Cell Modulation, Institute of Molecular Embryology and Genetics; [b]Department of Clinical Chemistry and Informatics, Graduate School of Pharmaceutical Sciences; [c]Department of Pediatrics, Graduate School of Medical Sciences, and [f]Department of Dermatology and Plastic Surgery, Faculty of Life Sciences; [i]Division of Reproductive Engineering, Center for Animal Resources and Development, Kumamoto University, Kumamoto, Japan; [d]Department of Neurology, Neuro-uscular Center, National Omuta Hospital, Omuta, Fukuoka, Japan; [e]Department of Pediatrics, Saga University, Faculty of Medicine, Saga, Japan; [g]DNAVEC Corporation, 6 Ookubo, Tsukuba, Ibaragi, Japan; [h]Precursory Research for Embryonic Science and Technology (PRESTO), Japan Science and Technology Agency (JST), Kawaguchi, Saitama, Japan

Correspondence: Takumi Era, Ph.D., M.D., Department of Cell Modulation, Institute of Molecular Embryology and Genetics, Kumamoto University, 2-2-1 Honjo, Chuo-ku, Kumamoto 860-0811, Japan. Telephone: 81-96-373-6589; Fax: 81–96-373-6590; e-mail: tera@kumamoto-u.ac.jp or Tetsumi Irie, Ph.D., Department of Clinical Chemistry and Informatics, Graduate School of Pharmaceutical Sciences, Kumamoto University, 5-1 Oe-honmachi, Chuo-ku, Kumamoto 862–0973, Japan. Telephone: 81-96-371-4552; Fax: 81-96-371-4552; e-mail: tirie@gpo.kumamoto-u.ac.jp.

Received June 13, 2014; accepted for publication October 31, 2014; first published online in STEM CELLS EXPRESS December 17, 2014.

1066-5099/2014/$30.00/0

http://dx.doi.org/10.1002/stem.1917

Key Words. Induced pluripotent stem cells • Transgene-free • Niemann-Pick disease type C • Experimental models

ABSTRACT

Niemann-Pick disease type C (NPC) is a lysosomal storage disease characterized by abnormal accumulation of free cholesterol and glycolipids. Here, we established induced pluripotent stem cell (iPSC) lines from NPC patients. Hepatocyte-like cells (HLCs) and neural progenitors derived from the iPSC lines accumulated cholesterol and displayed impaired autophagy and ATP production. A molecular signature related to lipid metabolism was also impaired in the NPC-iPSC-derived HLCs. These findings indicate that iPSC-derived cells can phenocopy human NPC. We also newly found that 2-hydroxypropyl-γ-cyclodextrin (HPGCD) could reduce the cholesterol accumulation and restore the functional and molecular abnormalities in the NPC patient-derived cells, and do so more effectively than 2-hydroxypropyl-β-cyclodextrin treatment. In addition, NPC model mice showed an improved liver status and prolonged survival with HPGCDs. Thus, iPSC lines derived from patient cells are powerful tools to study cellular models of NPC, and HPGCD is a potential new drug candidate for future treatment of this disease. STEM CELLS *2015;33:1075–1088*

INTRODUCTION

Induced pluripotent stem cells (iPSCs), which are artificially produced from human somatic cells, can be further induced to undergo sustained, unlimited growth, and exhibit multipotency (i.e., the ability to give rise to various cell types in vitro) [1, 2]. Because of these features, iPSCs are a potential source for cell therapy applications in clinical medicine. The process of iPSC generation, known as reprogramming, is triggered by the expression of four transcription factors, Oct3/4, Sox2, Klf4, and c-Myc, which are the same core factors underlying pluripotency in other pluripotent stem cells such as embryonic stem cells (ESCs) [3–5]. In particular, many procedures have now been reported to easily generate iPSCs from human fibroblasts and peripheral blood cells [6, 7].

Numerous iPSC lines derived from the somatic cells of patients harboring pathogenic mutations have been established and shown to phenocopy the disease [8–13]. These studies clearly demonstrated that disease-derived iPSC lines represent a powerful tool not only for cell therapy, but also for biomedical research and drug development [14, 15]. In particular, biomaterial samples obtained from patients with intractable diseases are indispensable for studying the underlying molecular mechanisms and developing new therapeutic agents. However, because the number and size of samples available from such patients are usually limited, disease-derived iPSCs are expected to be useful mainly as a replacement or supplemental source of biomaterials for developing new therapies.

Niemann-Pick disease type C (NPC) is a hereditary intractable disease associated with mutations in the lipid transporter genes, *NPC1* and *NPC2* [16, 17]. NPC1 helps to transport cholesterol between lysosomes and endoplasmic reticulum (ER) in cooperation with NPC2. Mutations in the *NPC1* and *NPC2* genes disrupt this transporting system, resulting in the accumulation of free cholesterol and glycolipids in lysosomes [18]. NPC patients suffer from liver and neurological dysfunctions and eventually die due to respiratory and hepatic failure [18]. Miglustat is a lipogenesis inhibitor indicated for NPC; however, its effect is so limited that patients eagerly await new advances in drug development for NPC therapy [19].

Our work aims to generate iPSC lines from patients with NPC to establish a disease model mirroring the cellular phenotype of NPC, and then use this model to screen drug candidates. To generate the iPSC lines from NPC patients safely and efficiently, we took advantage of the SeV vector that does not integrate into host genomes and can easily provide transgene-free iPSC lines. In this study, we generated iPSC lines from NPC skin fibroblasts, and found that subsequently derived hepatocyte-like cells (HLCs) and neural progenitors accumulate free cholesterol and exhibit functional defects. Using this system, we tested three types of cyclodextrin drugs for their ability to reduce the cholesterol accumulation. Interestingly, in addition to 2-hydroxypropyl-β-cyclodextrin (HPBCD), we newly found that 2-hydroxypropyl-γ-cyclodextrin (HPGCD) could remove the free cholesterol accumulated in NPC-derived HLCs and neural progenitors and restore the functionality of the HLCs. Moreover, liver dysfunction and cholesterol accumulation in NPC model mice were markedly improved with the HPGCD treatment. Dose-loading tests also showed that HPGCD is much safer than HPBCD. Our findings confirm the potential value of NPC-derived iPSC lines for studying cellular models of disease and highlight HPGCD as a future drug candidate for NPC.

Materials and Methods

iPSC Generation

iPSCs were generated from human skin-derived fibroblasts as described previously [20]. Briefly, 5×10^5 cells of human fibroblast cells per well of six-well plate were seeded 1 day before infection and then were infected with Sendai virus (SeV) vectors at 10 multiplicity of infection. After 7 days of culturing for fibroblasts, the infected cells were harvested by trypsin and replated at 5×10^4 cells per 60-mm dish on mitomycin C-treated mouse embryonic fibroblast feeder cells. From 18 to 25 days after infection, colonies were picked and recultured in human iPSC medium. To remove Sendai virus, the temperature of culture was shifted from 37°C to 38°C for 3 days at passage 1 or 2 of the iPSCs. Other materials and methods are described in Supporting Information Materials and Methods.

Results

Establishment of Disease-Derived iPSC Lines

To establish a cellular model of NPC, we attempted to generate iPSC lines from skin fibroblasts of two patients carrying different *NPC1* mutations. The efficiency of iPSC generation from these patients was similar to that from healthy volunteers, suggesting that *NPC1* mutations do not affect the efficiency of cell reprogramming (Supporting Information Fig. S1A). The NPC fibroblast-derived iPSCs exhibited ESC-like morphology and expressed a set of pluripotent markers (Fig. 1A; Supporting Information Fig. S1B, S1C). The nested PCR that can detect a single positive cell among 1 million cells confirmed a free of SeV contamination (Supporting Information Fig. S1B, S1D). We then investigated the differentiation potential of our NPC-derived iPSCs by evaluating teratoma formation. Histological analysis revealed that the teratomas analyzed comprised descendants of all three germ cell layers such as cuboidal epithelia, melanin pigment-containing cells, cartilage, muscle, and various glandular structures (Supporting Information Fig. S1E). The NPC iPSC lines had a normal karyotype, 46XY and 46XX, and mutations in the *NPC1* gene were confirmed by DNA sequencing (Supporting Information Fig. S1F, S1G). Thus, the NPC-derived iPSCs fulfilled the criteria for iPSC lines.

Morphological and Functional Analyses of NPC-Derived iPSC Lines

Liver enlargement is a major symptom of NPC patients, and those with severe forms of the disease suffer from liver dysfunction and failure [18]. To investigate the effect of Npc1 deficiency on the hepatocytic lineage, we differentiated NPC-derived iPSC lines into HLCs expressing albumin. We previously demonstrated that treatment with Activin A selectively induces the differentiation of mouse ESCs into definitive endoderm cells and HLCs, and that an endodermal surface marker, Cxcr4, could be used to detect endodermal differentiation [21, 22]. Thus, in this study, we similarly directed the iPSC lines into endodermal and hepatic lineages (Supporting Information Fig. S2A). On day 18 of differentiation, the HLCs expressed α-fetoprotein (~65% of total cells), albumin (~80% of total cells), and other hepatic markers (Supporting Information Fig. S2B, S2C); they also absorbed indocyanine green (ICG) and stored glycogen (Supporting Information Fig. S3A). The generation rate of definitive endoderm-like cells, calculated as the percentage of Cxcr4-positive cells (Supporting Information Fig. S3B), and the efficiency of hepatic differentiation, calculated from the percentage of albumin-positive cells and the marker expressions (Fig. 1B; Supporting Information Fig. S2C), were similar between the normal cell- and NPC-derived iPSC lines. In contrast, the NPC-derived HLCs were larger than the control HLCs (Fig. 1C). In NPC patients, defective transportation of cholesterol from lysosomes to ER results in the accumulation of free cholesterol in lysosomes [18]. Therefore, we used filipin staining, which specifically detects free cholesterol in cells, to assess the level of cholesterol accumulation. We observed negligible numbers of positively stained cells in the control HLCs derived from healthy volunteers, whereas the NPC-derived HLCs showed extreme levels of cholesterol accumulation (Fig. 1D), suggesting that these cells mirror the cellular phenotype of NPC.

Next, we investigated the various functions of HLCs generated from normal and NPC-derived iPSC lines. We could not detect any differences in terms of ICG uptake or release, glycogen storage, albumin production, urea secretion, or ammonia removal, all of which are indicative of hepatocyte function (Supporting Information Fig. S3A, S3C–S3E). The ATP levels in NPC-HLCs were significantly lower than those in control HLCs (Fig. 1E), although apoptosis in the NPC-HLCs was not exacerbated compared to that in the controls (Supporting Information Fig. S3F, S3G). To investigate the membrane potential of mitochondria, we used the specific MitoTracker staining reagents, JC-1 and CMXRos [23, 24]. JC-1 concentrates in the mitochondria and aggregates at normal mitochondrial membrane potentials, resulting in a high red/green fluorescence intensity ratio. Reduced mitochondrial membrane potential affects the aggregation of JC-1, resulting in a decreased red/green fluorescence intensity ratio. In addition, CMXRos

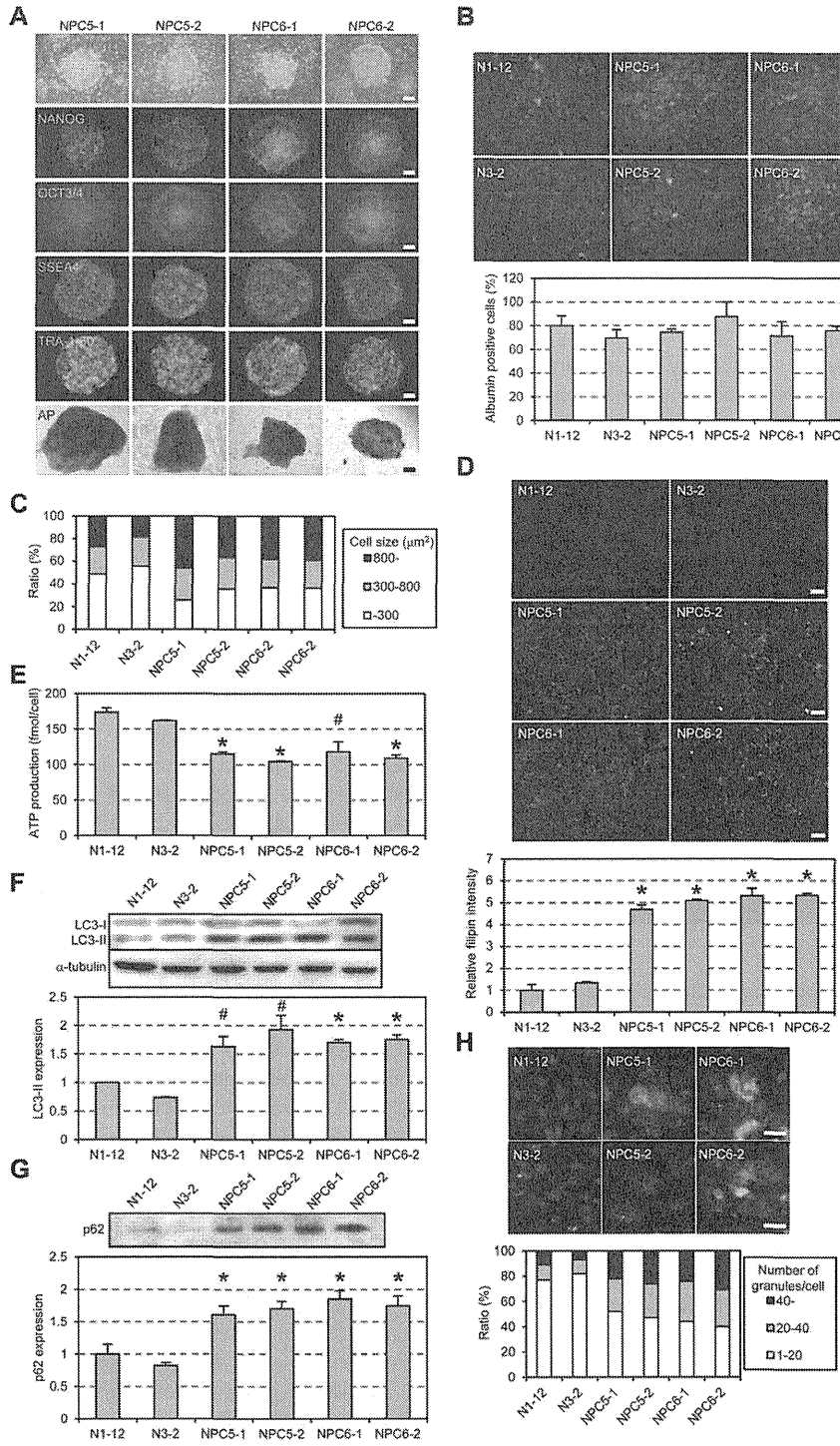

Figure 1. A cellular model of NPC using NPC-derived induced pluripotent stem cells (iPSCs). **(A):** Phase contrast images, immunofluorescence, and AP staining of iPSC lines for pluripotency markers. The iPSC lines NPC5-1 and −2, and NPC6-1 and −2, were derived from the NPC patients, NPC5 and NPC6, respectively. Scale bars = 200 μm. **(B):** Albumin expression in normal and NPC-derived hepatocyte-like cells (HLCs). Representative images of immunostaining for albumin (green) and propidium iodide staining of nuclei (blue) are shown in the upper panels. The bar graph in the lower panel shows the means ± SD of three independent experiments. The proportion of albumin-positive cells in differentiated NPC-derived iPSC lines was similar to that in the normal control. Scale bars = 100 μm. **(C):** Cell size of HLCs. The cell size of albumin-positive cells in Figure 1B was calculated using IN CELL ANAYZER 6000 (GE Healthcare). The NPC-derived HLCs were larger than normal HLCs. **(D):** Cholesterol accumulation in HLCs derived from NPC-iPSC lines. Free cholesterol was examined by filipin staining (upper image), and the relative intensity was calculated relative to the normal iPSC line, N1–12 (lower graph). Data are means ± SD of three independent experiments. NPC-derived HLCs showed a marked and significant accumulation of free cholesterol compared with HLCs derived from the normal iPSC lines, N1–12 and N3-2. *, $p < .01$, indicated NPC-iPSC line versus normal iPSC lines, Student's t test. Scale bars = 100 μm. **(E):** ATP levels in HLCs derived from iPSC lines. Experiments were conducted in triplicate (mean ± SD). The ATP levels were significantly lower in NPC-derived HLCs than in normal controls. *, $p < .01$; #, $p < .05$, indicated NPC-iPSC line versus normal iPSC lines, Student's t test. **(F):** Autophagy was upregulated and the protein levels of LC3-II were significantly elevated in NPC-derived HLCs. *, $p < .01$; #, $p < .05$, indicated NPC-iPSC lines versus normal iPSC lines, N1–12, and N3-2, Student's t test. The expression level was normalized to the expression of α-tubulin in each iPSC line. **(G):** Impairment of autophagic flux in NPC-derived HLCs. The insoluble form of p62 was enhanced in NPC-derived HLCs compared with that in normal HLCs. **(H):** Immunofluorescence staining for p62. Abnormal aggregation of p62 was strongly present in NPC-derived HLCs (green, upper panel). The aggregated granules were counted and the results summarized in the lower graph. The proportion of cells carrying more than 40 granules was increased in NPC-derived HLCs compared to normal HLCs. Nuclear staining, Hoechst 33258 (blue); scale bars = 25 μm. Abbreviations: AP, alkaline phosphatase; NPC, Niemann-Pick disease type C.

accumulates in mitochondria at normal membrane potential. We could not detect any difference in staining patterns for JC-1 or CMXRos between normal and NPC-derived HLCs (Supporting Information Fig. S3H, S3I).

Cellular autophagy is impaired in lysosomal storage diseases [25], therefore we used two methods to monitor the autophagy pathway in our NPC-derived HLCs compared to controls. First, we examined expression of the autophagy marker, microtubule-associated protein 1 light chain 3 (LC3) (Fig. 1F) [26]. C-terminal processing of LC3 produces LC3-I, which is modified to LC3-II with the initiation of autophagosome formation. We also measured p62/SQSTM1 (p62) expression to assess autophagic flux (Fig. 1G, 1H) [27]. Because p62 binds to LC3 and is degraded upon fusion with the lysosome, impairment of autophagy flux results in the accumulation and aggregation of insoluble p62. The expression levels of LC3-II and insoluble p62 proteins were higher in NPC-HLCs than in normal HLCs (Fig. 1F, 1G). In addition, the NPC-derived HLCs showed excessive p62 aggregation compared with normal HLCs (Fig. 1H). These results suggested that autophagy is upregulated and autophagic flux is impaired in the NPC-derived HLCs.

Effect of Various Cyclodextrin Treatments on Cholesterol Accumulation and Restoration of Cellular Functions

A major aim of generating iPSCs from NPC patient cells is to develop an in vitro system for screening drug candidates. Our observation of extreme cholesterol accumulation in NPC iPSC-derived HLCs prompted us to examine the effect of various drug treatments on this process; specifically, we tested a series of 2-hydroxypropyl-cyclodextrins of different cavity sizes. 2-Hydroxypropyl-β-cyclodextrin (HPBCD) is effective for reducing cholesterol accumulation in *NPC1*-defective cells [28], and this was supported by our findings of significantly reduced cholesterol accumulation in NPC-HLCs with HPBCD treatment (Fig. 2A). Interestingly, 2-hydroxypropyl-α-cyclodextrin (HPACD) had no effect on cholesterol accumulation, while HPGCD reduced the cholesterol accumulation in NPC-HLCs to the same extent as HPBCD (Fig. 2A). The size of HLCs was also decreased by the treatments with HPBCD and HPGCD (Supporting Information Fig. S4A). Notably, low concentrations (100 μM) of HPBCD and HPGCD were ineffective for reducing cholesterol accumulation (Supporting Information Fig. S4B). The cholesterol accumulation does not appear before day 11 of the culture (Fig. 2B). In contrast, it is greatly and significantly enhanced on day 14, comparing to the control, and continuously increased up to day 22 during the hepatic differentiation. The 4-day treatments of HPBCD and HPGCD from day 18 to day 22 can significantly reduce the accumulation (Fig. 2B).

We next examined when during hepatic differentiation HPBCD and HPGCD are effective in reducing the NPC phenotype. By drug-treating our HLCs at various time points, we found that HPBCD and HPGCD effectively reduced cholesterol accumulation during the last 4 days (days 15–18) of hepatic differentiation (Fig. 2C). From days 15 to 18, differentiating HLCs express α-fetoprotein and albumin, and before day 15 the cells are intermediates between hepatic cells and iPSCs (Supporting Information Fig. S2B, S2C). These results therefore indicated that HPBCD and HPGCD could impede the cholesterol accumulation of NPC-derived cells at the hepatic cell stage in the in vitro iPSC cultures.

We next asked whether the cyclodextrin treatments could restore the abnormally low ATP levels and abnormal autophagy exhibited by the NPC-derived HLCs, and found that HPBCD and HPGCD treatment recovered both these functional abnormalities (Fig. 2D–2F; Supporting Information Fig. S4C).

NPC patients suffer from neural dysfunction [29], thus we examined whether neural cells derived from NPC-iPSCs also accumulate free cholesterol and if such a defect could be abrogated by HPGCD treatment. Neural progenitors expressing nestin were induced from healthy donor- and NPC-derived iPSCs and tested for marker expression during the neural differentiation. The expressions of the neural progenitor markers were gradually elevated in both normal and NPC-derived iPSC lines, whereas pluripotent markers such as Oct3/4 and Nanog were markedly decreased up to day 7 (Fig. 3A; Supporting Information Fig. S5A). These results suggest that the differentiation potential into neural progenitors in NPC-derived iPSC lines is almost equal to that in normal iPSC lines. However, the NPC-derived neural progenitors exhibited cholesterol accumulation that was significantly reduced with HPBCD and HPGCD treatments (Fig. 3B, 3C). Similar to NPC-derived HLCs, we found the low ATP levels and the abnormal autophagy which were restored with HPBCD and HPGCD treatments (Fig. 3D, 3E). HPBCD and HPGCD did not affect the levels of neural marker expression (Supporting Information Fig. S5B). These results indicated that both HLCs and neural cells derived from NPC-iPSCs are useful for evaluating drug candidates and that HPGCD, in addition to HPBCD, is a promising drug candidate for NPC treatment. Taken together, our data validate transgene-free iPSC lines as cellular models for NPC.

HPBCD and HPGCD Have a Different Effect on the Cholesterol Accumulation from Miglustat

Miglustat is used to treat NPC patients [30]. We next investigated the effect of Miglustat on the cholesterol accumulations in iPSC-derived neural progenitors and HLCs. Although HPGCD and HPBCD treatment could reduce the accumulations in both the cells, Miglustat could not at all remove the cholesterol accumulation from the cells with 4-day treatments (Fig. 4A). Similarly, neither ATP level nor abnormal autophagy were restored in both the cells with the Miglustat treatments (Fig. 4B, 4C; Supporting Information Fig. S6A, S6B). These results are reasonable because Miglustat is an enzyme inhibitor for glycosylceramide synthase, and suggest that the action mechanism of HPGCD and HPBCD is different from that of Miglustat [31]. We confirmed that Miglustat treatment could inhibit the glycosyl-ceramide synthesis in the iPSC-derived cells (Fig. 4D; Supporting Information Fig. S6C).

HPGCD Treatment Restores the Molecular Abnormalities More Effectively than HPBCD Treatment

We then used microarray analysis to further characterize the NPC-derived HLCs. A large number of genes were differentially expressed in each NPC-derived HLC line compared with healthy donor-derived HLCs, including 361 datasets of commonly downregulated and 362 datasets of commonly upregulated genes with a fold change >1.5 (Fig. 5A). To elucidate the functional significance of these changes in gene expression, we analyzed the commonly downregulated and

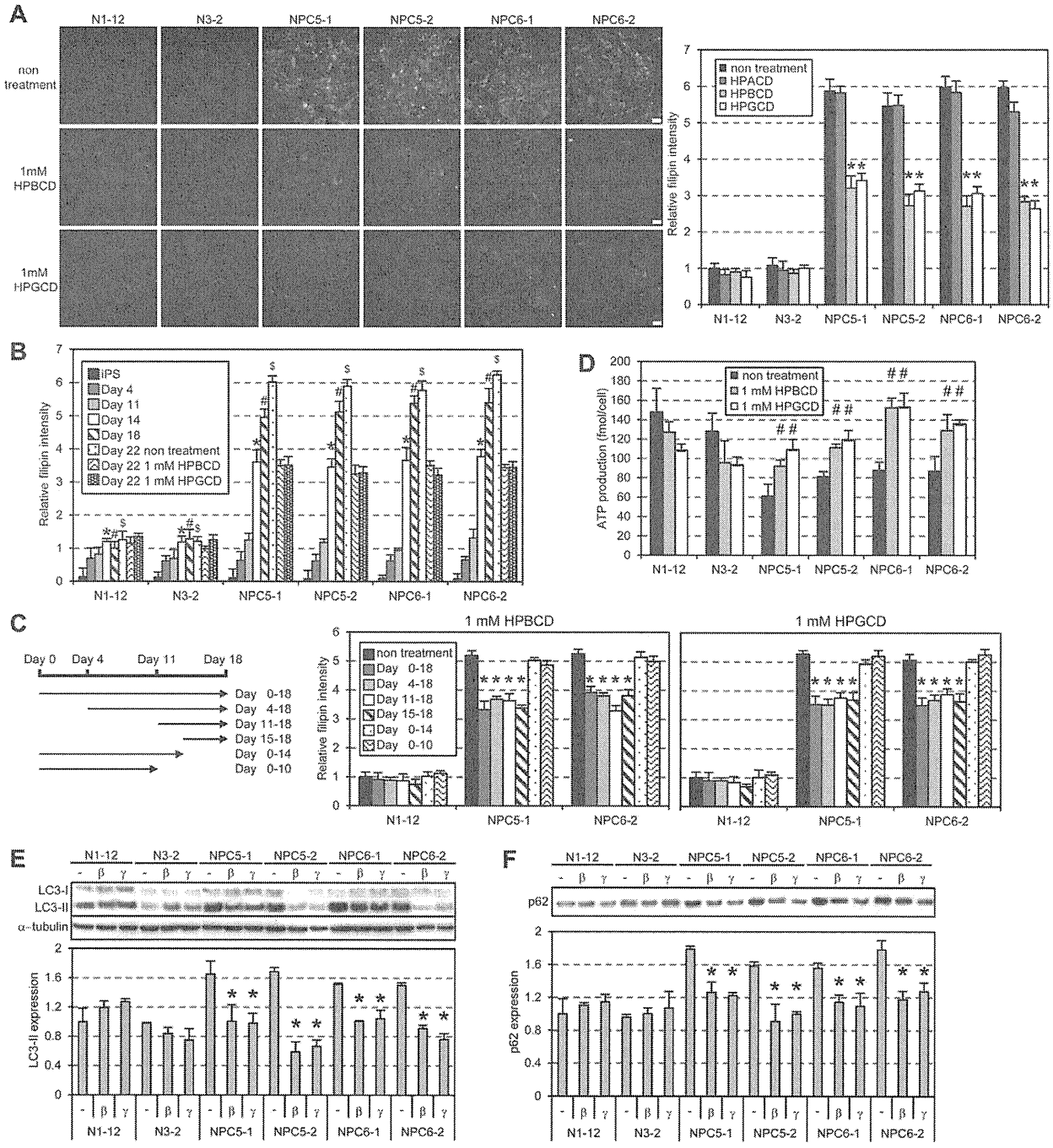

Figure 2. Effect of cyclodextrins on cholesterol accumulation in NPC-derived hepatocyte-like cells (HLCs). **(A):** Effect of a series of hydroxypropyl-cyclodextrins on the reduction of free cholesterol accumulation in NPC-derived HLCs. HLCs were cultured with 1 mM of the indicated hydroxypropyl-cyclodextrin for 4 days, filipin stained (left image), and analyzed with an IN Cell Analyzer (right graph, GE Healthcare). Data are means ± SD of three independent experiments. HPGCD and HPBCD, but not HPACD, significantly reduced free cholesterol accumulation in the NPC-derived HLCs. *, $p < .01$, nontreatment versus treatment of each NPC-derived HLC, Student's t test. Scale bars = 50 μm. **(B):** The free cholesterol accumulation during the hepatic differentiation. The filipin staining data were analyzed with an IN Cell Analyzer. The cells were treated with HPBCD and HPGCD from day 18 to day 22. Experiments were conducted in triplicate (mean ± SD). *, #, $, $p < .01$, NPC clones versus normal clones, Student's t test. **(C):** Effects of HPBCD and HPGCD on the reduction of free cholesterol accumulation in NPC-derived induced pluripotent stem cell (iPSC) differentiation. The differentiated iPSCs were treated with 1 mM of HPBCD or HPGCD for the indicated times (left panel). The filipin staining data were analyzed with an IN Cell Analyzer (right graph). HPBCD and HPGCD treatments were effective at hepatic stages from day 15 to day 18 during in vitro iPSC differentiation. Experiments were conducted in triplicate (mean ± SD). *, $p < .01$, nontreatment versus treatment, Student's t test. **(D):** HPBCD and HPGCD treatments restored ATP levels of HLCs derived from NPC-iPSC lines. The levels were significantly recovered by treatments with HPBCD and HPGCD. HLCs were culture with 1 mM 2-hydroxypropyl-cyclodextrins (HPCDs) for 4 days. Data are means ± SD of three independent experiments. #, $p < .05$, nontreatment versus treatment, Student's t test. **(E):** HPCD treatments restored the abnormal induction of autophagy in NPC-derived HLCs. The expression level of LC3 was recovered to normal levels by treatments with HPBCD and HPGCD. β: Treatment with 1 mM HPBCD for 4 days, γ: 1 mM HPGCD treatment for 4 days. The expression level was normalized to α-tubulin expression in each iPSC line. **(F):** HPCD treatments restored the impairment of autophagic flux. HPBCD and HPGCD treatments reduced the amount of insoluble p62 in NPC-derived HLCs. β: Treatment with 1 mM HPBCD for 4 days, γ: 1 mM HPGCD treatment for 4 days. Abbreviations: HPACD, 2-hydroxypropyl-α-cyclodextrin; HPBCD, 2-hydroxypropyl-β-cyclodextrin; HPGCD, 2-hydroxypropyl-γ-cyclodextrin; NPC, Niemann-Pick disease type C.

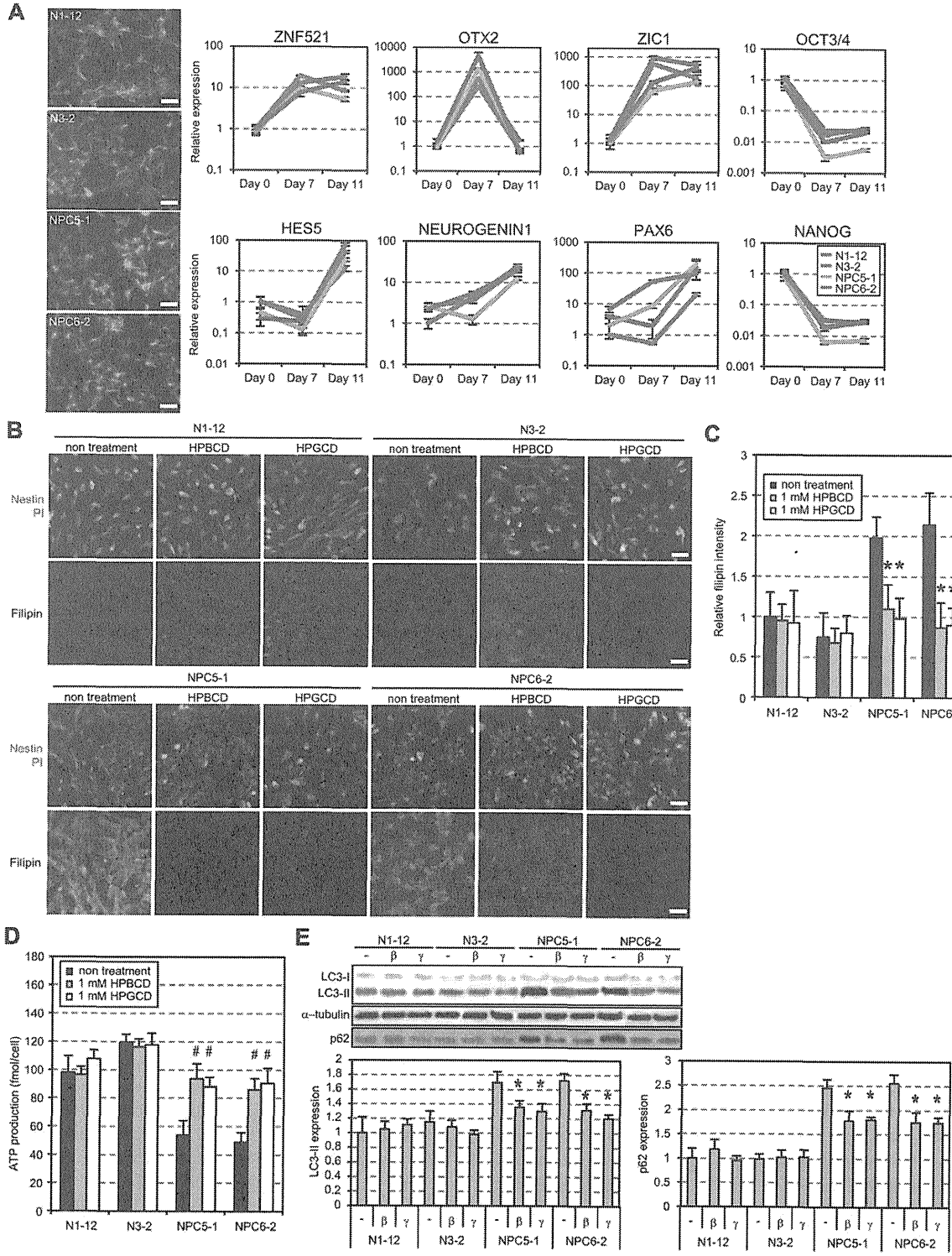

Figure 3. Effect of cyclodextrins on cholesterol accumulation in neural progenitors. **(A):** Marker expressions of neural progenitors derived from the induced pluripotent stem cell (iPSC) lines. The neural progenitors were induced from healthy donor- and NPC-derived iPSC lines. The cells showed expressed nestin (left panel, immunostaining) as well as other neural progenitor markers (right panel, qPCR). Scale bars = 50 μm. **(B, C):** Effect of HPBCD and HPGCD on the reduction of free cholesterol accumulation in NPC-derived neural progenitors. Neural progenitors were cultured with 1 mM of the indicated hydroxypropyl-cyclodextrin for 4 days, filipin, nestin and PI stained (B), and analyzed with an IN Cell Analyzer (C). Data are means ± SD of three independent experiments. HPGCD and HPBCD treatments significantly reduced free cholesterol accumulation in the nestin^{+} NPC-derived neural progenitors. *, $p < .01$, nontreatment versus treatment of each NPC-derived neural progenitors, Student's t test. Scale bars = 50 μm. **(D):** HPBCD and HPGCD treatments restored ATP levels of NPC-derived neural progenitors. The neural progenitors were culture with 1 mM 2-hydroxypropyl-cyclodextrins (HPCDs) for 4 days. Data are means ± SD of three independent experiments. #, $p < .05$, nontreatment versus treatment, Student's t test. **(E):** HPCD treatments restored the abnormal autophagy in NPC-derived neural progenitors. The expression levels of LC3 (upper and left lower panels) and p62 (upper and right lower panels) were decreased by treatments with HPBCD and HPGCD. β: Treatment with 1 mM HPBCD for 4 days, γ: 1 mM HPGCD treatment for 4 days. The expression level was normalized to α-tubulin expression in each iPSC line. Abbreviations: HPBCD, 2-hydroxypropyl-β-cyclodextrin; HPGCD, 2-hydroxypropyl-γ-cyclodextrin; NPC, Niemann-Pick disease type C; PI, propidium iodide.

upregulated genes identified using gene set enrichment analysis (GSEA). Analysis of the commonly downregulated genes revealed the following four molecular signatures to be significantly altered in NPC-derived HLCs compared to normal control cells: lipid metabolism, biosynthesis, cellular lipid metabolism, and cellular transport ($p < .05$; Fig. 5B). Among the 1,972 genes related to lipid metabolism, 10 genes were identified as downregulated by GSEA (HSD17B3, FSHB, ACACB, NAPEPLD, NR2F2, UGT2B15, PCYT1B, DGKE, APOC3, and CCL5) (Fig. 5C). Similarly, 46 and 34 genes related to biosynthesis and cellular transport, respectively, were identified as downregulated, and of these, 6 biosynthesis-related and 3 transport-related genes overlap with those related to lipid metabolism, while, 6 genes related to cellular lipid metabolism are absolutely included in the gene set related to lipid metabolism. Next, we investigated the effects of HPBCD and HPGCD on the expressions of genes included in the abnormal molecular signatures. The cluster analysis revealed that treatment of the cells with HPGCD shifted all the functionally related gene expression patterns closer to the normal patterns than treatment with HPBCD (Fig. 5C). Conversely, one molecular signature related to protein metabolism was identified among the commonly upregulated genes ($p < .05$; Fig. 5B); however, neither cyclodextrin treatment efficiently shifted this gene expression pattern toward that of the normal cells (Supporting Information Fig. S7A, Table S5). Taken together, the results indicated that lipid and protein metabolic processes are impaired in NPC-derived HLCs and that they are more effectively improved by HPGCD treatment than HPBCD treatment.

Molecular Signatures Altered with HPGCD Treatment Are Different from Those with HPBCD Treatment

To further characterize the HPBCD and HPGCD effects on NPC-derived HLCs, we analyzed gene expression profiles from the microarray experiments. The patterns of global gene expression were similar between untreated HLCs and cells treated with HPBCD (Fig. 5D; Supporting Information Fig. S7B), but different with HPGCD treatment (Fig. 5E; Supporting Information Fig. S7C). Interestingly however, there were differences in specific gene expression patterns between HPGCD-treated and HPBCD-treated HLCs, suggesting that HPGCD and HPBCD have different effects on iPSC-derived HLCs at the molecular level (Fig. 5F; Supporting Information Fig. S7D). Further GSEA to explore the functional significance of changes in gene expression with HPGCD and HPBCD treatments revealed the specific molecular signatures in the commonly downregulated genes in NPC-derived HLCs (Fig. 5A). The one molecular signatures significantly altered by the HPBCD treatment relate functionally to immunity ($p < .05$; Fig. 5G). HPGCD treatment significantly changed gene expression patterns related to three molecular signatures ($p < .05$; Fig. 5G). The molecular signatures related to chemical stimulus response and cell-cell signaling were significantly identified in the HPGCD-treated cells, but not in the HPBCD-treated cells. In the top-10 signatures, some molecular signatures such as lipid metabolism were affected by both cyclodextrin treatments (Fig. 5G). The cluster analysis revealed that HPGCD treatment shifted HPBCD-altered signature with $p < .05$ closer to the normal pattern than HPBCD (Supporting Information Fig. S7E). However, HPGCD-altered signature with $p < .05$, as shown in Figure 5G, did not show this tendency (Supporting Information Fig. S7E). We also analyzed the top-10 signatures together. Interestingly, while HPGCD treatment shifted HPGCD-altered signatures closer to the normal pattern than HPBCD, HPBCD treatment shifted the HPBCD-altered signatures closer to the normal pattern than HPGCD (Supporting Information Fig. S7F). We attempted to enrich the molecular signatures identified in the commonly upregulated genes of HLCs derived from NPC-iPSC lines, but found no effect with either HPBCD or HPGCD treatment. The fact that some molecular signatures were common and others specifically and significantly changed by HPGCD treatment only suggests that the molecular mechanisms underlying the cholesterol reduction are different between HPBCD and HPGCD treatments, although they share some common mechanisms. The results of DNA arrays were confirmed by quantitative RT-PCR of the genes that were randomly selected from the heatmap (Supporting Information Figs. S8–S11).

HPGCD Treatment Can Improve NPC-Model Mice

Herein we identified a novel effect of HPGCD on the reduction of cholesterol accumulation in NPC-derived HLCs. Next, we asked whether HPGCD treatment could be similarly effective in NPC model mice bearing a spontaneous mutation of the *Npc1* gene that causes a defect in lysosome to ER trafficking of cholesterol. These mice also exhibit a similar phenotype to the human disease including cholesterol accumulation in the liver and brain. The model mice show liver injury and neural functional impairment and die before 12 weeks old without proper treatment [32].

We treated 4-week-old NPC mice with HPGCD once a week until 8.5 weeks of age (Fig. 6A) by subcutaneous injection (five injections in total). Following treatment, aspartate aminotransferase and alanine aminotransferase, serum markers for liver injury, were markedly and significantly reduced (Fig. 6B), and histological analysis revealed a marked morphological improvement in the livers of mice treated with HPGCD (Fig. 6C). Vacuolization and lipid-laden macrophages observed in the livers of saline-treated NPC mice were almost absent in the treated mice (Fig. 6C; Supporting Information Fig. S12A). Consistently, the free cholesterol accumulation was significantly decreased in the livers of the HPGCD-treated mice, compared to those of saline-treated mice (Fig. 6D). Interestingly, Purkinje cells of HPGCD-treated mice still partially remained in the cerebellar vermis, comparing to the saline-treated NPC mice (Fig. 6E; Supporting Information Fig. S12A), suggesting that HPGCD injection affects both liver and cerebellar defects in the NPC model mice.

Cellular markers of autophagy such as LC3-II and insoluble p62 were upregulated in the livers and brains of saline-treated NPC mice, and then significantly reduced with the HPGCD treatment (Fig. 6F), indicating that HPGCD could also recover autophagy function in the liver and brain of NPC model mice.

Survival analysis shows that the HPGCD treatment could significantly prolong the NPC mouse survival by 10–14 days (Fig. 6G). To clarify the cause of death in the treated mice, we carefully and extensively examined the pathology of the organs such as heart, lung, liver, kidney, and cerebellum in the dead mice. Many vacuoles were observed in the liver and kidney of the saline-treated mice, suggesting that free cholesterol and glycolipids are accumulated in them (Fig. 6H;

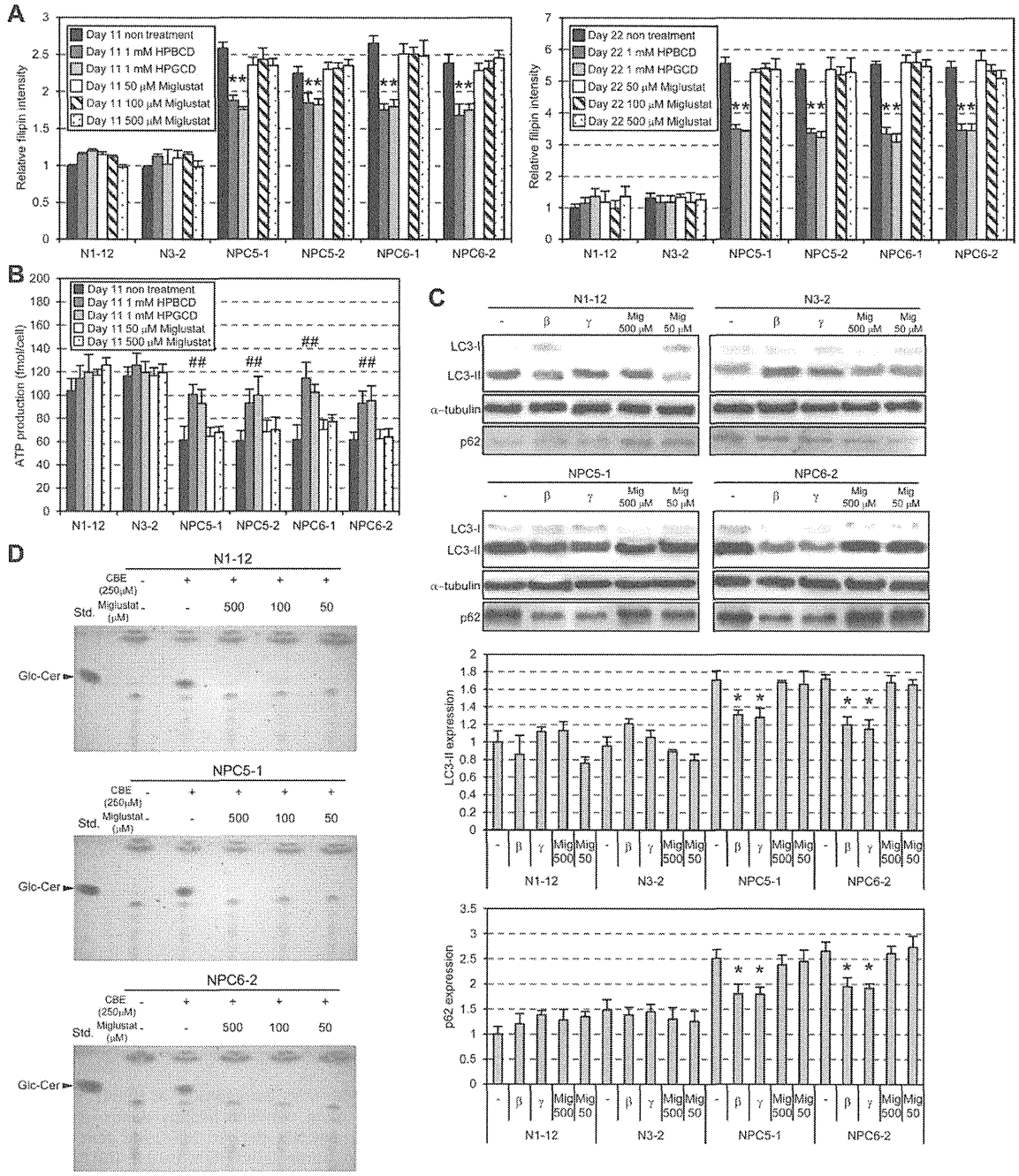

Figure 4. Action mechanism of 2-hydroxypropyl-cyclodextrin (HPCD) is different from Miglustat. **(A):** Effect of Miglustat on the free cholesterol accumulation in the NPC-derived cells. Neural progenitors (left graph) and hepatocyte-like cells (right graph) were cultured with the various concentration of Miglustat and 1 mM of the indicated hydroxypropyl-cyclodextrin for 4 days, filipin stained, and analyzed with an IN Cell Analyzer. Miglustat did not reduce the cholesterol accumulation. Data are means ± SD of three independent experiments. *, $p < .01$, nontreatment versus treatment of each NPC-derived cells, Student's t test. **(B):** HPBCD and HPGCD but not Miglustat treatments restored ATP levels of NPC-derived neural progenitors. The levels were significantly recovered by treatments with HPBCD and HPGCD. Data are means ± SD of three independent experiments. #, $p < .05$, nontreatment versus treatment, Student's t test. **(C):** HPCD but not Miglustat treatments restored the abnormal autophagy in NPC-derived neural progenitors. The expression levels of LC3 and p62 were decreased by treatments with HPBCD and HPGCD. In contrast, Miglustat did not affect the expression levels of LC3 and p62. β: Treatment with 1 mM HPBCD for 4 days, γ: 1 mM HPGCD treatment for 4 days, Mig: Treatment with the indicated concentration of Miglustat for 4 days. The expression level was normalized to α-tubulin expression in each iPSC line. **(D):** Miglustat can inhibit the synthesis of glycosylceramide in NPC-derived neural progenitors. The glycosylceramide expression disappeared with Miglustat treatment, suggesting that Miglustat inhibit the synthesis of glycosylceramide by blocking the activity of glycosylceramide synthase. Abbreviations: CBE, conduritol B epoxide, inhibitor of β-glucocerebrosidase; Glc-Cer, glycosylceramide; HPBCD, 2-hydroxypropyl-β-cyclodextrin; HPGCD, 2-hydroxypropyl-γ-cyclodextrin; NPC, Niemann-Pick disease type C; Std, glycosylceramide as a standard.

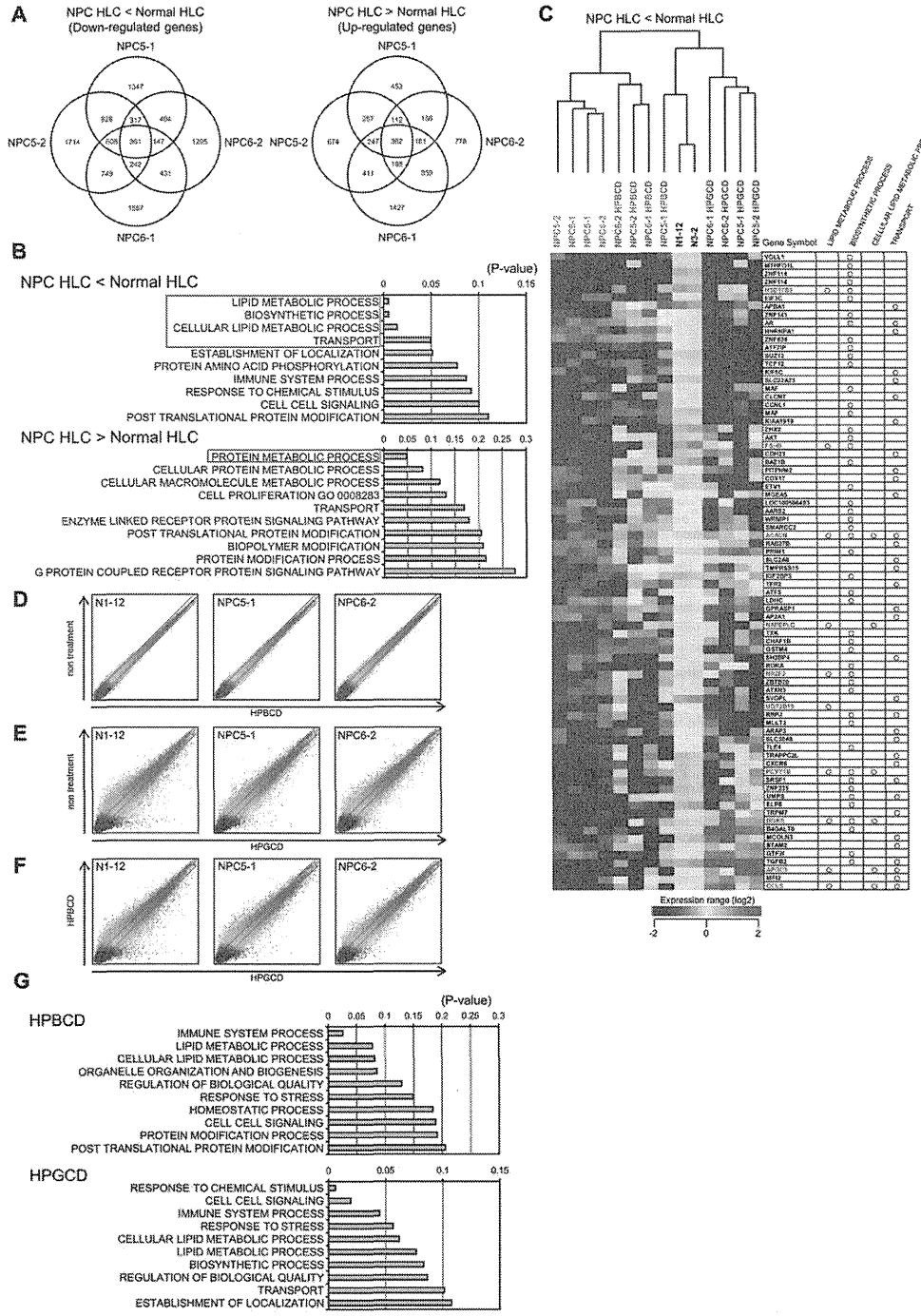

Figure 5. Characterization of HLCs derived from the induced pluripotent stem cell (iPSC) lines with HPGCD or HPBCD treatments. **(A):** Venn diagram for the genes that were downregulated or upregulated by 1.5-fold or more between healthy donor- and NPC-derived HLCs. Comparing downregulated or upregulated gene profiles between healthy donor- and NPC-derived HLCs, the gene expressions of 361 datasets were commonly downregulated (left panel) and those of 362 datasets were upregulated (right panel). **(B):** Molecular signatures were altered in NPC-derived HLCs. Gene set enrichment analysis (GSEA) enriched the biological processes of gene ontology, which are significantly altered in NPC-derived HLCs. The molecular signatures in the red squares were significantly ($p < .05$) changed in NPC-derived HLCs, compared to healthy donor-derived HLCs. Upper graph: downregulated signatures in NPC, lower graph: upregulated signatures in NPC. **(C):** Hierarchical clustering of genes significantly downregulated in NPC. The datasets of the genes included in the molecular signatures as shown in the red square of Figure 5B were clustered according to Euclidean distance metrics. The datasets of NPC-derived HLCs with HPGCD treatment (blue) were close to those of normal HLCs (black). In contrast, the datasets of NPC-derived HLCs (pink) and three out of four with HPBCD treatments (green) were classified into the separate branch from those of normal HLCs. The genes selected are classified into the four signatures: lipid metabolic process, biosynthetic process, cellular lipid metabolic process, and transport (right panel). Red gene names indicate those genes included in the Lipid metabolic process. **(D–F):** Global gene-expression patterns of the HLCs following HPBCD and HPGCD treatments. Scatter-plot representations of the global gene-expression patterns for HLCs in the presence and absence of HPBCD (D) or HPGCD (E) were compared. In addition, scatter-plot representations of the global gene-expression patterns for the HLCs with HPGCD treatment were compared to those with HPBCD treatment (F). The pattern of global gene expression for HLCs with HPGCD treatment is different from that with no treatment or HPBCD treatment. N1–12 and N3-2: HLCs derived from normal iPSC lines; NPC5-1, NPC5-2, NPC6-1, and NPC6-2: HLCs derived from NPC-iPSC lines. **(G):** Some molecular signatures specifically altered with HPGCD treatment differed from those altered with HPBCD treatment. In the commonly downregulated genes in NPC-derived HLCs (Fig. 5A), GSEA enriched the biological processes containing the genes that were significantly changed with HPBCD (upper) or HPGCD (lower) treatments. The molecular signatures including response to chemical stimulus and cell signaling were specifically and significantly altered with HPGCD treatment ($p < .05$). Abbreviations: HLC, hepatocyte-like cell; HPBCD, 2-hydroxypropyl-β-cyclodextrin; HPGCD, 2-hydroxypropyl-γ-cyclodextrin; NPC, Niemann-Pick disease type C.

Supporting Information Fig. S12B). In contrast, the organs of the HPGCD-treated mice look normal with no vacuoles. However, the defect of Purkinje cells in the cerebellum was exacerbated and was not at all improved even with the HPGCD treatment (Fig. 6I; Supporting Information Fig. S12B). Consistently, the cholesterol accumulation was not reduced in the brain of HPGCD-treated mice (Supporting Information Fig. S12C). Based on these results, we concluded that HPGCD-treated mice died due to the neurological disturbance.

Finally, we examined the toxic effects of HPBCD and HPGCD in vitro and in vivo. HPGCD was much less toxic than HPBCD in both iPSC-derived HLCs and normal mice (Fig. 7A, 7B). Indeed, high-dose HPBCD treatment decreased cell viability and mouse survival rate, whereas similar doses of HPGCD had no effect on cell viability and mouse survival rate. Interestingly, the NPC-derived HLCs showed less toxicity to HPBCD treatment than normal HLCs (Fig. 7A). These data suggest that HPGCD is a safer candidate than HPBCD for NPC therapy in the future. Taken together, our results indicate that HPGCD treatment can improve the abnormalities in NPC model mice and that HPGCD is a potential drug candidate for NPC treatment.

Discussion

We established iPSC lines from two patients with NPC and demonstrated that these lines provide an appropriate cellular model of the disease. Using the model, we found a new drug candidate, HPGCD, for NPC therapy.

Our finding that free cholesterol accumulated in HLCs and neural progenitors derived from NPC-iPSC lines was consistent with the cholesterol accumulation observed in the livers and brains of NPC patients [18]. Biochemical analysis revealed low ATP production and abnormal autophagy in the NPC-derived HLCs and neural progenitors compared with the normal controls. These low ATP levels are consistent with the abnormally low levels of ATP observed in the brain, muscle, and liver of 9-week-old *Npc1*-null mice [33], and although we found no differences in the mitochondrial membrane potentials, the low ATP levels also suggested that reduced mitochondrial activity in HLCs and neural progenitors is an early event of NPC. Reduction in mitochondrial activity occurs in the early phases of apoptosis, as detected in the liver tissue of adult *Npc1* null mice (more than 7 weeks old), but not young *Npc1* null mice (less than 7 weeks old) [34]. Here, we found no evidence of enhanced apoptosis in NPC-HLCs newly generated from NPC-derived iPSC lines, suggesting that cellular apoptosis is not a feature of the early disease phase, despite the cholesterol accumulation.

Both HLCs and neural progenitors derived from NPC-iPSCs showed elevated protein levels of LC3-II and insoluble p62, as well as abnormal p62 aggregation, compared to those derived from normal controls. LC3-II is a robust marker for autophagy induction, and impairment of autophagic flux is associated with accumulation of insoluble p62, which forms abnormal aggregates [26, 27]. Therefore, our results suggest that the *NPC1* mutation in the iPSC-derived HLCs and neural progenitors caused both induction of autophagy and impairment of autophagic flux. Abnormal autophagic events are widely observed in lysosomal storage diseases [25], and a marked accumulation of autophagosomes is observed in the liver tissues of *Npc1*-null mice and fibroblasts of NPC patients [35, 36]. Taken together, our results therefore suggested that both reduced ATP levels and enhanced autophagy induction are early pathogenic events of NPC.

In this study, GSEA revealed that lipid and protein metabolism were significantly impaired in NPC-derived HLCs. Cholesterol and glycosphingolipids are key molecules in the pathogenesis of NPC, and previous studies implicated molecular pathways related to lipid metabolism in the liver and brain abnormalities observed in NPC mice [34, 37]. However, because these previous results were obtained from the tissues and organs of NPC mice, it could not be determined whether the pathways were directly affected by the NPC mutation or were secondary effects to tissue destruction processes such as inflammation. Moreover, it is still unclear whether cyclodextrin treatments can restore the abnormal molecular pathways observed in NPC cells. In this study, HPBCD treatment reduced cholesterol accumulation in NPC-iPSC-derived HLCs and neural progenitors. This result confirms and extends the previous findings that HPBCD treatment effectively reduces cholesterol accumulation in *Npc1*-null mice and NPC-derived fibroblasts [38–40].

We newly found that HPGCD treatment also effectively reduced cholesterol accumulation in NPC-derived HLCs and neural progenitors, but that HPACD had no effect. In addition, both HPBCD and HPGCD restored ATP levels and abnormal autophagy in NPC-derived HLCs and neural progenitors, and HPGCD treatment dramatically improved liver injury and abnormal autophagy in NPC mice, as well as prolonging survival. Moreover, cerebellar Purkinje cell defects in the model mice were partially improved with HPGCD treatment. Previous study demonstrated that HPBCD could not enter the central nervous system (CNS) through the blood brain barrier (BBB) in normal and NPC model mice. However, a volume of distribution available to HPBCD exceeded the accepted values for plasma and vascular volume of the brain, indicating a considerable cell surface binding of HPBCD to the endothelium of the cerebral vasculature. This may provide a favorable influence to normalize the biochemical and morphological abnormality of CNS in NPC model mice [41]. In a similar manner to HPBCD, the molecular weight of HPGCD (1,668 Da) prevents it from transiting the BBB. The mechanism underlying the effect on the cerebellar Purkinje cell is still unclear and further studies are needed to elucidate it.

Although the HPGCD treatment with the subcutaneous injection prolonged the mice survivals, the treated mice finally died due to the neurological disturbance. Histological analyses could not find any marked abnormality in the lung, heart, kidney, and liver of the HPGCD-treated mice. These results suggest that HPGCD treatment is effective on the major organs except for the CNS. The intrathecal injection of HPGCD should be considered to treat the neurological disturbance of NPC mice.

HPACD, HPBCD, and HPGCD consist of six, seven, and eight D-glucopyranose units, respectively, linked to 2-hydroxypropyl groups by α-1,4 glycosidic bonds to form a macrocycle [42]. This structure provides the cyclodextrins with a hydrophilic outer surface and a somewhat hydrophobic central cavity. The ability of each hydroxypropyl-cyclodextrin to form inclusion complexes with specific guest molecules

depends upon the cavity size. For instance, the acyl chain of phospholipids fits tightly into the small hydrophobic cavity of HPACD, whereas the side chain of cholesterol is preferentially included in the larger inner space of the HPBCD and HPGCD cavities [43]. Thus, our observation that HPBCD and HPGCD, but not HPACD, were effective in reducing cholesterol

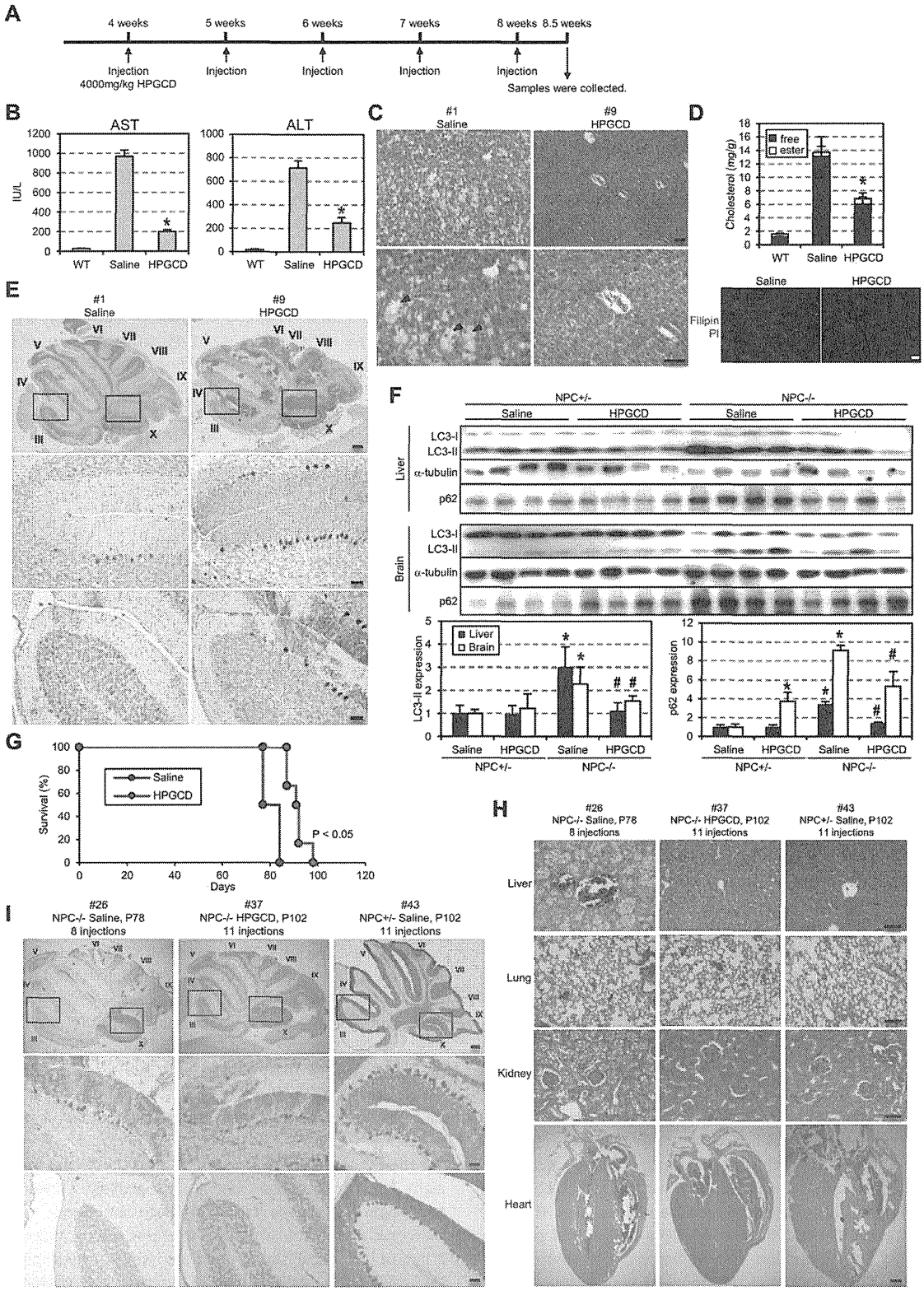

Figure 6.